Computing the steady states for an asymptotic model of quantum transport in resonant heterostructures

Virginie Bonnaillie-Noël, Francis Nier, Mamodyasine Patel

Computing the steady states for an asymptotic model of quantum transport in resonant heterostructures

Virginie Bonnaillie-Noël*, Francis Nier* and Yassine Patel *
IRMAR, UMR-CNRS 6625, Université de Rennes I, 35042 Rennes Cedex, FRANCE

Abstract

In this article we propose a rapid method to compute the steady states, including bifurcation diagrams, of resonant tunneling heterostructures in the far from equilibrium regime. Those calculations are made on a simplified model which takes into account the characteristic quantities which arise from an accurate asymptotic analysis of the nonlinear Schrödinger-Poisson system. After a summary of the former theoretical results, the asymptotical model is explicitly adapted to physically realistic situations and numerical results are shown in various cases.

MSC : 34L25, 34L30, 34L40, 65L10, 65Z05, 82D37

Keywords : Schrödinger-Poisson system, resonant tunneling diode, asymptotic model

Acknowledgements.
The authors would like to thank N. Ben Abdallah, F. Mehats, C. Presilla, J. Sjöstrand, O. Vanbésien and B. Vinter for remarks and discussions about this work. They were partly supported by the french ACI n° 1034 "Systèmes hors-équilibre quantiques et classiques".

1 Introduction.

Over the past twenty years there has been a serious effort to develop efficient numerical methods in order to compute the steady states of out of equilibrium quantum resonant heterostructures. The final aim is to be able to predict from numerical simulations the I-V characteristic curve for devices which involve an unusual coupling between spectral quantities associated with the quantum mechanics and nonlinear effects due to the electrostatic mean field. Two types of models were considered : purely quantum ones based on Schrödinger-Poisson systems or Wigner-Poisson systems (see for example [1, 2, 3, 4, 5, 6, 30, 34, 35]); and quantum hydrodynamic or drift- diffusion models (see for example [9, 10, 11, 13, 36]). The second ones which assume local thermal equilibrium or local entropy maximizing states are well suited for situations where quantum effects, averaged by the statistics over a large number of particles, only bring small corrections to classical mechanics. The first ones on which we will focus stick to the quantum nature of the phenomena and have to be chosen in order to describe accurately the quantum transport. Actually both of those models were able to recover the negative differential resistance typical of resonant tunneling diodes. This phenomenon which is essentially a linear phenomenon

*Email adresses: Virginie.Noel-Bonnaillie@univ-rennes1.fr, Francis.Nier@univ-rennes1.fr, Patel@univ-rennes1.fr

relies on the basic topological argument that, when the bias is increased, the resonant energy eventually crosses the ground energy of the incoming beam. It is therefore very robust, remains in all the considered models and survives to any numerical discretization. The situation became more complicated after the work by Jona-Lasinio, Presilla and Sjöstrand, [21, 37], where they showed that the Schrödinger-Poisson system could lead to hysteresis phenomena in agreement with physical observations. Other works mentioned the possibility of having much more complex bifurcation diagrams [22]. In order to catch all these phenomena, an accurate treatment of the tunnel effect through the barrier has to be taken into account and one has to start with quantum models like Schrödinger-Poisson of Wigner-Poisson systems rather than hydrodynamical models. A first difficulty which has to be taken into account is related with the out of equilibrium regime. At the quantum level it can be done in the Landauer-Büttiker ([8, 25]) approach directly on the Schrödinger-Poisson system or via the Wigner-Poisson system ([12, 14, 24]). This has motivated several theoretical studies concerned with the numerical treatment of artificial boundary conditions ([1, 2]), with the well posedness of the nonlinear problem ([5, 6, 30]) and with the derivation of asymptotic models ([21, 31, 32, 33, 37]). The second difficulty comes from the complexity of a rough numerical treatment due to the presence of resonant states. The system requires a spatial and a spectral discretization. But resonances lead to very stiff spectral quantities (with slopes like $e^{\frac{C}{h}}$, $h << 1$) which require a specific treatment. It can be done via WKB techniques and this was accurately done in [21] and implemented in numerical methods by N. Ben Abdallah and O. Pinaud in [7, 34, 35]. However the numerical complexity remains still large enough in order to motivate the derivation of simplified model which would permit a rapid insight of possible bifurcation diagrams.

In [21, 37], it is suggested that hysteresis phenomena occur only when the drain barrier is thicker or higher than the source one. Therefore the geometry of the barriers is an important parameter and it is actually an unknown affected by the nonlinearity even when this nonlinearity is not very large. The analysis carried out by the third author on the specific asymptotic model of quantum wells in a semiclassical island was developed in order to elucidate the role of the geometry of the barriers in these nonlinear phenomena. It has been done in a general enough framework in order to cover several heterostructure problems. In doing so, he provided the right quantities which govern the nonlinear phenomenon with an accurate treatment of the tunnel effect. Here we present an adaptation of the theoretical asymptotic analysis which leads to a very rapid determination of bifurcation diagrams.

The outline of the article is the following :

1. Model : In this section, we present the nonlinear Schrödinger-Poisson problem with the Landauer-Büttiker approach which involves the stationnary scattering states.

2. Scaling : We introduce the natural reference magnitudes of this problem. Three numerical dimensionless parameters h, β and γ arise from the scaling of the equations.

3. Theoretical results : The results obtained in [32, 33] are summarized in the specific regime $h \to 0$.

4. Validity of the asymptotic model : On complete numerical computations for the original model, we check that the theoretical asymptotic model in the limit $h \to 0$ is relevant.

5. Implementation of the asymptotic model : A distinction is made here between the quantities which are taken out of the asymptotic model and the ones which are computed exactly.

6. Computation of the Agmon distances : This short section provides exact analytical expressions for quantities which are involved in the final algorithm.

7. Penalization method : Several cases have to be considered. They are separated by multidimensional non convex constraints. Their implementation is done via a penalization method which is specified in this section.

8. Numerical results : Several numerical results are shown for AlGaAs-GaAs or Si-Si0 structures, with a possible comparison with existing numerical results.

9. Conclusion.

10. Appendix, Critical cases with two wells : Some detailed calculations for the asymptotic model are provided there.

2 The model.

In resonant tunneling diodes and similar heterostructures, the electronic transport occurs transversally to the heterojunctions. It is modelled with a one dimensional system in the direction $\underline{x} = \underline{x}_3$ which involves mean or integrated quantities along the 2-dimensional parallel direction $(\underline{x}_1, \underline{x}_2)$. The mass m that we use, is the effective electronic mass $m = m_3$ in the direction $\underline{x} = \underline{x}_3$.
The quantum hamiltonian for a single electron has the form

$$\frac{\hbar^2}{2m} D_{\underline{x}}^2 + \underline{\mathcal{V}}(\underline{x}), \quad D_{\underline{x}} = \frac{1}{i}\partial_{\underline{x}}, \quad \underline{\mathcal{V}} = \underline{\mathcal{B}} + \underline{\mathcal{V}}_0 + \underline{V}_{NL}, \tag{2.1}$$

with a nonlinear potential $\underline{V}_{NL}$ which is non negative and takes into account the mean repulsive electrostatic field inside the device. It is assumed that these nonlinear effects are negligible (quasineutral approximation) outside the device and we will come back to this point in our conclusion (Section 10). The potential $\underline{\mathcal{V}}$ is the total potential in the device. The first potential term $\underline{\mathcal{B}}$ simply includes the bias voltage applied to the device. It is piecewise affine

$$\underline{\mathcal{B}}(\underline{x}) = -\underline{B}\left[\frac{\underline{x}-a}{b-a} 1_{[a,b]}(\underline{x}) + 1_{[b,+\infty)}(\underline{x})\right].$$

The second term describes the barriers and the wells,

$$\underline{\mathcal{V}}_0(\underline{x}) = \underline{V}_0 1_{[a,b]}(\underline{x}) + \sum_{j=1}^{N} \underline{W}_j(\underline{x}),$$

with the constant $\underline{V}_0 > 0$ and the compactly supported potentials $\underline{W}_j \in L^\infty(\mathbb{R})$, $-\underline{V}_0 \le \underline{W}_j \le 0$, fixed. The external potential $\underline{\mathcal{B}} + \underline{\mathcal{V}}_0$ is represented in Figure 1.

The shape of the incoming beam of electrons is contained in the prescribed function $\underline{f}$. For the initial presentation, we focus on the case of a beam coming from the left-hand side and described by a function $\underline{f}$ supported in $\underline{k} \ge 0$. The more physically relevant case where the injection comes from both sides will be discussed further in Section 4.4. We assume that the injection profile is governed by the thermodynamic equilibrium

$$\underline{f}(\underline{k}) = \underline{g}(\underline{k}^2) 1_{\mathbb{R}_+}(\underline{k}), \quad \text{with} \quad \underline{g}(\underline{k}^2) = \frac{\sqrt{m_1 m_2}\, k_B T}{\pi\hbar^2} \ln\left(1 + \exp\left(\frac{E_F - \frac{\hbar^2 \underline{k}^2}{2m}}{k_B T}\right)\right), \tag{2.2}$$

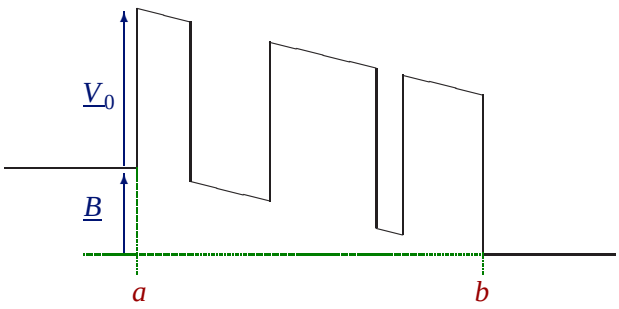

Figure 1: Representation of the external potential in the device

where $\underline{g}$ represents the Fermi-Dirac distribution function after integration along the two directions $(\underline{x}_1, \underline{x}_2)$ with $\underline{x} = \underline{x}_3$, and E_F is the Fermi level given by

$$E_F = \frac{\hbar^2}{2} \left(3\pi^2 n_D\right)^{2/3} \left(m_1 m_2 m_3\right)^{-1/3} .$$

Here the introduction of a non isotropic effective electronic mass (m_1, m_2, m_3) permits to apply our model and numerical simulation to heterostructures like Si-SiO. The symbol n_D denotes the donor density outside the device ($\underline{x} \notin [a,b]$).
The out-of-equilibrium regime for Schrödinger-Poisson system requires the introduction of the generalized eigenfunctions in order to describe the steady state density. For a prescribed incoming flow, one uses the incoming generalized eigenfunctions $\underline{\psi}_-(\underline{k},\underline{x})$ defined for $\underline{k} > 0$ by

$$-\frac{\hbar^2}{2m}\frac{d^2}{d\underline{x}^2}\underline{\psi}_-(\underline{k},\underline{x}) + \underline{\mathcal{V}}\underline{\psi}_-(\underline{k},\underline{x}) = \frac{\hbar^2\underline{k}^2}{2m}\underline{\psi}_-(\underline{k},\underline{x}), \quad \text{for } \underline{x} \in \mathbb{R}, \tag{2.3}$$

$$\underline{\psi}_-(\underline{k},\underline{x}) = \mathrm{e}^{i\underline{k}\underline{x}} + R(\underline{k})\,\mathrm{e}^{-i\underline{k}\underline{x}} \quad \text{for } \underline{x} \le a \quad \text{and} \quad \underline{\psi}_-(\underline{k},\underline{x}) = T(\underline{k})\,\mathrm{e}^{i\sqrt{\underline{k}^2+\underline{B}}\,\underline{x}} \quad \text{for } \underline{x} \ge b .$$

The particle density $\underline{n}$ is then defined by

$$\forall \phi \in \mathcal{C}_c^0((a,b)), \int_a^b \underline{n}(\underline{x})\phi(\underline{x})d\underline{x} = \int_0^{+\infty} \underline{g}(\underline{k}^2) \int_a^b |\underline{\psi}_-(\underline{k},\underline{x})|^2 \phi(\underline{x})d\underline{x}\,\frac{d\underline{k}}{2\pi} = Tr[\underline{f}(K)\phi]. \tag{2.4}$$

Finally the nonlinear potential $\underline{V}_{NL}$ satisfies the Poisson equation

$$\begin{cases} -\Delta \underline{V}_{NL} = \dfrac{q^2}{\varepsilon}\underline{n}, \\ \underline{V}_{NL}(a) = \underline{V}_{NL}(b) = 0. \end{cases} \tag{2.5}$$

3 Scaling the equation.

In order to make precisely the connection with the theoretical analysis and for a more flexible numerical treatment (which can be adapted to several semiconductors), the Schrödinger-Poisson system is written here with dimensionless quantities and unknowns. This writing also permits to identify the small parameter.

3.1 Schrödinger equation.

The reference length and energy will be the total length of the device $L = b - a$ and the Fermi level E_F. With the change of variables $x = \frac{\underline{x}-a}{L}$, we define the new functions

$$u(x) = \underline{u}(Lx+a) = \underline{u}(\underline{x}) \quad \text{and} \quad \mathcal{V}^h(x) = \frac{1}{E_F}\underline{\mathcal{V}}(Lx+a) = \frac{1}{E_F}\underline{\mathcal{V}}(\underline{x}).$$

The equation

$$-\frac{\hbar^2}{2m}\frac{d^2}{d\underline{x}^2}\underline{u} + \underline{\mathcal{V}}\,\underline{u} = \frac{\hbar^2\underline{k}^2}{2m}\underline{u},$$

becomes

$$-\frac{\hbar^2}{2mL^2E_F}\frac{d^2}{dx^2}u + \mathcal{V}\ u = \frac{\hbar^2k^2}{2mE_F}u.$$

The new dimensionless wave vector is given by

$$k = \frac{\hbar}{\sqrt{2mE_F}}\underline{k},$$

while our semiclassical parameter, supposed to be small and which is actually reasonnably small in applications, will be

$$h = \frac{\hbar}{\sqrt{2mE_F}}\frac{1}{L} = \frac{L_F}{L}\,.$$

Note that the quantity $L_F = \hbar/\sqrt{2mE_F}$ represents the Fermi length. Therefore, the equation (2.3) is rewritten

$$-h^2\frac{d^2}{dx^2}u + \mathcal{V}^h\ u = k^2u\,.$$

We write $\mathcal{V}^h$ in the form

$$\mathcal{V}^h(x) = \frac{1}{E_F}\underline{\mathcal{V}}(\underline{x}) = \mathcal{B}(x) + \mathcal{V}_0^h(x) + V_{NL}^h(x)\,,$$

where

$$\mathcal{B}(x) = \frac{1}{E_F}\underline{\mathcal{B}}(\underline{x}) = -B\left[x\,1_{[0,1]}(x) + 1_{[1,+\infty)}(x)\right], \quad \text{with} \quad B = \frac{\underline{B}}{E_F}\,,$$

$$V_{NL}^h(x) = \frac{1}{E_F}\underline{V}_{NL}(\underline{x})\,,$$

and

$$\mathcal{V}_0^h(x) = V_0\ 1_{[0,1]}(x) + \sum_{j=1}^{N} W_j\left(\frac{x-c_j}{h}\right), \quad \text{with} \quad W_j\left(\frac{x-c_j}{h}\right) = \frac{1}{E_F}\underline{W}_j(\underline{x}), \quad V_0 = \frac{\underline{V}_0}{E_F}\,.$$

For $h > 0$, it is always possible to define $W_j(y) = E_F^{-1}\underline{W}_j(L(c_j + hy))$. The writing $W_j(\frac{x-c_j}{h})$ suggests that the j-th well concentrates at $x = c_j$ when $h > 0$ is small. The theoretical analysis was carried out in this specific framework by Patel in [32] in the limit $h \to 0$. Actually, this scaling was motivated by the fact that the heterostructures present a finite number of resonant states in the relevant energy interval. The asymptotic of quantum wells $W_j(\frac{x-c_j}{h})$ in a semiclassical island $\mathcal{B}(x) + V_{NL}^h(x) + V_0 1_{[0,1]}(x)$ permits to keep this constraint even in the limit $h \to 0$. The points c_j can be thought as averaged positions in the wells. They are not exactly the middle points and their determination in practical situations with $h > 0$ will be described in Subsection 6.1.

3.2 Fermi-Dirac function.

In order to rescale the Fermi-Dirac function $\underline{g}$, we set $\beta = \dfrac{E_F}{k_B T}$, then

$$\begin{aligned} \underline{g}(\underline{k}^2) &= \frac{\sqrt{m_1 m_2}k_B T}{\pi\hbar^2} \ln\left(1+\exp\left(\frac{E_F - \frac{\hbar^2\underline{k}^2}{2m}}{k_B T}\right)\right) \\ &= \frac{\sqrt{m_1 m_2}k_B T}{\pi\hbar^2} \ln\left(1+\exp(\beta(1-k^2))\right). \end{aligned}$$

The function g is then defined by introducing the rescaled energy k^2 :

$$g(k^2) = \frac{\pi\hbar^2}{\sqrt{m_1 m_2}E_F}\underline{g}(\underline{k}^2) = \beta^{-1}\ln\left(1+\exp(\beta(1-k^2))\right).$$

3.3 Generalized eigenfunctions.

With the condition $\min W_j \geq -V_0$, the hamiltonian $H^h = -h^2\Delta + \mathcal{V}^h$ has only absolute continuous spectrum (see [32] and references therein). The injection profile in 1-dimension is given by function of the asymptotics momentum according to [6, 14, 30]. It is written in terms of the generalized eigenfunctions as

$$f(K_-^h)(x,x') = \int_{-\infty}^{+\infty} f(k)\psi_-^h(k,x)\overline{\psi_-^h(k,x')}\frac{dk}{2\pi h}. \tag{3.1}$$

After the scaling, those generalized eigenfunctions are defined according to :

$k > 0$

$$\begin{aligned} H^h\psi_-^h(k,x) &= k^2\psi_-^h(k,x), \\ \psi_-^h(k,x) &\sim e^{ikx/h} + R(k)\,e^{-ikx/h} \quad \text{for} \quad x \to -\infty, \\ \psi_-^h(k,x) &\sim T(k)\,e^{i\sqrt{k^2+B}x/h} \quad \text{for} \quad x \to +\infty, \end{aligned}$$

$k < 0$

$$\begin{aligned} H^h\psi_-^h(k,x) &= (k^2-B)\psi_-^h(k,x), \\ \psi_-^h(k,x) &\sim e^{ikx/h} + R(k)\,e^{-ikx/h} \quad \text{for} \quad x \to +\infty, \\ \psi_-^h(k,x) &\sim T(k)\,e^{-i(k^2-B)^{1/2}x/h} \quad \text{for} \quad x \to -\infty. \end{aligned}$$

The complex square root $(z)^{1/2}$ chosen above as $(\rho e^{i\theta})^{1/2} = \sqrt{\rho}\,e^{i\theta/2}$ for $\rho \geq 0$ and $\theta \in [0, 2\pi)$.
In the case of a beam coming from the left-hand side with a Fermi-Dirac statistics g, the generalized eigenfunctions for the Hamiltonian H^h satisfy

$$f(K_-^h)(x,x') = \int_0^{+\infty} g(k^2)\psi_-^h(k,x)\overline{\psi_-^h(k,x')}\frac{dk}{2\pi h}.$$

An important remark in the analysis of [30, 32] says that the functions of the energy are specific functions of the momentum. Namely in terms of operator functional calculus, plugging $f(k) = F(k^2)1_{\{k>0\}} + F(k^2-B)1_{\{k<0\}}$ into (3.1) leads to $f(K_-^h) = F(H^h)$.

3.4 Density.

The electronic density is computed according to

$$\begin{aligned} L^3\underline{n}(\underline{x}) &= L^3\int_0^{+\infty}\underline{g}(\underline{k}^2)|\underline{\psi}_-(\underline{k},\underline{x})|^2\frac{d\underline{k}}{2\pi} \\ &= L^3\int_0^{+\infty}\frac{\sqrt{m_1m_2}E_F}{\pi\hbar^2}g(k^2)|\psi_-^h(k,x)|^2\frac{\sqrt{2mE_F}}{\hbar}\frac{dk}{2\pi} \\ &= L^2\frac{\sqrt{m_1m_2}E_F}{\pi\hbar^2}\int_0^{+\infty}g(k^2)|\psi_-^h(k,x)|^2\frac{dk}{2\pi h}. \end{aligned}$$

A natural definition of the rescaled density is

$$n(x) = \frac{\pi\hbar^2}{\sqrt{m_1m_2}E_F}L\underline{n}(\underline{x}).$$

3.5 Poisson equation.

To achieve the scaling, we now consider the Poisson equation. The nonlinear potential $\underline{V}_{NL}$ solves

$$-\frac{E_F}{L^2}\Delta V_{NL}^h(x) = -\Delta\underline{V}_{NL}(\underline{x}) = \frac{q^2}{\varepsilon}\underline{n}(\underline{x}) = \frac{q^2}{\varepsilon}\frac{1}{L}\frac{\sqrt{m_1m_2}\,E_F}{\pi\hbar^2}n(x).$$

Therefore, the rescaled nonlinear V_{NL}^h satisfies the equation

$$-\Delta V_{NL}^h(x) = L\frac{q^2\sqrt{m_1m_2}}{\varepsilon\pi\hbar^2}n(x).$$

3.6 Scaled system.

The previous normalizations are summarized in the rescaled system :

$$\left\{\begin{array}{l} -h^2\dfrac{d^2}{dx^2}\psi_-^h(k,x) + \mathcal{V}^h\psi_-^h(k,x) = k^2\psi_-^h(k,x), \quad \text{with boundary conditions,} \\ \mathcal{V}^h(x) = \mathcal{B}(x) + \mathcal{V}_0^h(x) + V_{NL}^h(x), \\ \mathcal{V}_0^h(x) = V_0 1_{[0,1]}(x) - \displaystyle\sum_{j=1}^N W_j\left(\frac{x-c_j}{h}\right), \\ g(k^2) = \beta^{-1}\ln\left(1+\exp(\beta(1-k^2))\right), \\ n(x) = \displaystyle\int_0^{+\infty}g(k^2)|\psi_-^h(k,x)|^2\frac{dk}{2\pi h}, \\ -\Delta V_{NL}^h = \gamma n, \quad \text{with} \quad V_{NL}^h(0) = V_{NL}^h(1) = 0, \end{array}\right. \tag{3.2}$$

where $x = \dfrac{\underline{x}-a}{L}$, $k = \dfrac{\hbar}{\sqrt{2mE_F}}\underline{k}$. The parameters equal

$$h = \frac{\hbar}{\sqrt{2mE_F}}\frac{1}{L} = \frac{L_F}{L}\,, \tag{3.3}$$

$$\beta = \frac{E_F}{k_B T} \quad \text{and} \quad \gamma = \frac{4L}{a_B}\,, \tag{3.4}$$

where the Bohr radius is defined as usual $a_B = \dfrac{4\pi\hbar^2\varepsilon}{\sqrt{m_1 m_2}\,q^2}$.

3.7 Current.

Although the current density is a final quantity which will always be presented in its physical units, we show for the sake of completeness how it can be rescaled in agreement with the previous choices. Before scaling, the current density $\underline{J}$ (up to the choice of sign) can be computed with the generalized eigenfunctions $\underline{\psi}_-(\underline{k},\underline{x})$ according to

$$L\underline{J} \;=\; \frac{e\hbar}{m}\int_0^{+\infty} \underline{g}(\underline{k}^2)\ \mathrm{Im}\left(\int_a^b \nabla\underline{\psi}_-(\underline{k},\underline{x})\overline{\underline{\psi}_-(\underline{k},\underline{x})}d\underline{x}\right)\frac{d\underline{k}}{2\pi}.$$

The introduction of the rescaled Fermi-Dirac function g and the comparison between the generalized eigenfunctions $\underline{\psi}_-$ and ψ_- lead to

$$\begin{aligned}\underline{J} \;&=\; \frac{e\hbar}{m}\frac{\sqrt{m_1m_2}E_F}{\pi\hbar^2}\frac{1}{L^2}\int_0^{+\infty} g(k^2)\ \mathrm{Im}\left(\int_0^1 \nabla\psi_-^h(k,x)\overline{\psi_-^h(k,x)}dx\right)\frac{dk}{2\pi h}\\ &=\; \frac{e\sqrt{m_1m_2}}{m}\frac{E_F}{\pi\hbar L^2}\int_0^{+\infty} g(k^2)\ \mathrm{Im}\left(\int_0^1 \nabla\psi_-^h(k,x)\overline{\psi_-^h(k,x)}dx\right)\frac{dk}{2\pi h}.\end{aligned}$$

This last expression allows to introduce the rescaled current J by

$$J = \int_0^{+\infty} g(k^2)\ \mathrm{Im}\left(\int_0^1 \nabla\psi_-^h(k,x)\overline{\psi_-^h(k,x)}dx\right)\frac{dk}{2\pi h}\,, \tag{3.5}$$

with the final relation $\underline{J} = \dfrac{e\sqrt{m_1m_2}}{m}\dfrac{E_F}{\pi\hbar L^2}\,J$.

4 Theoretical results.

This section gives a short account of the theoretical results which were obtained in [32] about the limit $h \to 0$ for the scaled system (3.2). After this presentation, it will be shown how the simple asymptotic model can be extended in order to include physically relevant situations.

4.1 Linear case.

Consider first a quantum Hamiltonian $H^h = -h^2 d^2/dx^2 + \mathcal{V}^h$ where the potential $\mathcal{V}^h$ is defined according to (3.2) with the nonlinear potential V_{NL}^h replaced by a non negative potential $V^h(x)$. Another change in the theoretical analysis is about the beam profile g which is replaced by a compactly supported function $\tilde{g}$.

Hypothesis 4.1. *The family $(V^h)_{h\in(0,1)}$ is assumed to be uniformly bounded in the space of Lipschitz functions $W^{1,\infty}([0,1])$ with a limit V in the $\mathcal{C}^0([0,1])$ topology.*

Hypothesis 4.2. *The function $\tilde{g}$ (which replaces the function g in (3.2)) is a continuous function with a compact support included in $[\Lambda_*,\Lambda^*]\subset(0,V_0-B)$. Moreover, the potentials W_j are compactly supported and satisfy $-V_0\le W_j\le 0$.*

Notation 4.3.

- *The potential $\tilde{\mathcal{V}}$ is the limiting filled (i.e. where the wells W_j have been removed) potential*

$$\tilde{\mathcal{V}}(x)=\mathcal{B}(x)+V_0 1_{[0,1]}(x)+V(x)\,.$$

- *For any $j=1,\dots,N$, the Schrödinger operator $H_j:=-d^2/dx^2+W_j(x)$, $D(H_j)=H^2(\mathbb{R})\subset L^2(\mathbb{R})$, admits a finite number of negative eigenvalues $(-\varepsilon_j^k)_{1\le k\le K_j<+\infty}$ labelled according to the increasing order. The set of energies $\mathcal{E}_j$ is defined by*

$$\mathcal{E}_j=\left\{\tilde{\mathcal{V}}(c_j)-\varepsilon_j^k,\ 1\le k\le K_j\right\}. \tag{4.1}$$

- *The quantities ε_j^k, $1\le k\le K_j$, $1\le j\le N$ are called the resonant depths.*

- *The set of resonant energies is defined as*

$$\mathcal{E}=\bigcup_{j=1}^{N}\mathcal{E}_j=\left\{\tilde{\mathcal{V}}(c_j)-\varepsilon_j^k,\ 1\le k\le K_j,\ 1\le j\le N\right\}. \tag{4.2}$$

- *For any $E\in\mathbb{R}$, we set*

$$J^E:=\{j\in\{1,\dots,N\}\quad s.t.\quad E\in\mathcal{E}_j\}.$$

  We say that the well c_j is resonant at the energy E when $j\in J^E$.

- *Finally, we set*

$$c_\ell^E:=\min_{j\in J^E}c_j,\quad c_r^E:=\max_{j\in J^E}c_j\,,$$

  and simply

$$c^E\quad \textit{when}\quad c_\ell^E=c_r^E\,.$$

Definition 4.4. *For $\Phi\in L^\infty([0,1];\mathbb{R})$, the Agmon distance is the degenerate distance given by*

$$d_{Ag}(x,y;\Phi)=\left|\int_x^y\sqrt{\Phi_+(t)}\,dt\right|,$$

with $\Phi_+(t)=\max\{\Phi(t),0\}$.
For a resonant energy $E\in\mathcal{E}$, we set

$$\delta_\ell^E:=d_{Ag}(c_r^E,1;\tilde{\mathcal{V}}-E)-d_{Ag}(0,c_r^E;\tilde{\mathcal{V}}-E),$$
$$\delta_r^E:=d_{Ag}(0,c_\ell^E;\tilde{\mathcal{V}}-E)-d_{Ag}(c_\ell^E,1;\tilde{\mathcal{V}}-E)\,.$$

Remark 4.5. *The Agmon distance is a standard tool in the analysis of WKB methods ([18]) and solves locally an Hamilton-Jacobi equation. It is usually referred to in the physics literature as the action.*

With this definition, $\delta_\ell^E > 0$ if and only if all the resonant wells at the energy E are in the left hand side of the island (i. e. closer to 0 than 1). Conversely, $\delta_r^E > 0$ if and only if all the resonant wells at the energy E are in the right hand side of the island (i. e. closer to 1 than 0). Actually, for $x,y \in [0,1]$, the distance with the asymptotic potential has to be thought as the limit

$$d_{Ag}(x,y;\tilde{\mathcal{V}} - E) = \lim_{h\to 0} d_{Ag}(x,y;\tilde{\mathcal{V}}^h - E) = \lim_{h\to 0} d_{Ag}(x,y;\mathcal{V}^h - E)\,.$$

Instead of writing explicitly a Theorem which would require additional technical (and sometimes artificial) mathematical assumptions, we simplify here the presentation of the results obtained in [31, 32]. We refer the reader to those references for more precise statements.

Result 1 : The electronic density defined by

$$n^h(x) = \int_0^{+\infty} \tilde{g}(k^2)\left|\psi_-^h(k,x)\right|^2 \frac{dk}{2\pi h}\,,$$

defines a non negative measure in $[0,1]$ which admits weak* limit points in the set $\mathcal{M}_b([0,1])$ of bounded Radon measures on $[0,1]$ as $h \to 0$. By assuming Hypothesis 4.1 and Hypothesis 4.2, those limit points take the form in $]0,1[$

$$\mu\big|_{]0,1[}(x) = \sum_{E\in\mathcal{E}} \sum_{j\in J^E} t_j^E\, \tilde{g}(E)\, \delta_{c_j}(x)\,,$$

where the coefficients t_j^E satisfy

$$t_j^E \in [0,1] \quad \text{and} \quad \left\{ \begin{array}{lcl} \delta_\ell^E > 0 & \Rightarrow & t_j^E = 1,\ \forall j \in J^E, \\ \delta_r^E > 0 & \Rightarrow & t_j^E = 0,\ \forall j \in J^E. \end{array} \right. \tag{4.3}$$

Generic case : The non degenerate case is when $\#J^E = 1$ with $\delta_\ell^E > 0$ or $\delta_r^E > 0$ for all $E \in \mathcal{E} \cap \operatorname{supp}\tilde{g}$. Then the sequence $n^h\big|_{]0,1[}$ admits a unique limit point :

$$n^h\big|_{]0,1[}(x) \overset{h\to 0}{\rightharpoonup} \sum_{E\in\mathcal{E}} 1_{\delta_\ell^E>0}(E)\, \tilde{g}(E)\, \delta_{c^E}(x)\,.$$

Critical case 1 : Already with one resonant state, $\mathcal{E} \cap \operatorname{supp}\tilde{g} = \{E_0\}$ with $\#J^{E_0} = 1$, a non generic case may appear. It corresponds to the case $\delta_\ell^{E_0} = \delta_r^{E_0} = 0$:

$$d_{Ag}(0,c^{E_0};\tilde{\mathcal{V}} - E_0) = d_{Ag}(c^{E_0},1;\tilde{\mathcal{V}} - E_0)\,. \tag{4.4}$$

It was shown that this asymptotic information on the Agmon distances (it is written in terms of the asymptotic potential $\tilde{\mathcal{V}}$) does not prevent any value $t_1^{E_0} \in [0,1]$. Note that the indeterminacy of $t_1^{E_0}$ is replaced by the constraint (4.4).

Critical case 2 : Another interesting case which is considered by our numerical calculations, is about the case $\#J^{E_0} = 2$ (for the sake of simplicity we assume here again $\mathcal{E} \cap \operatorname{supp}\tilde{g} = \{E_0\}$). First, since E_0 is a limiting resonant energy (i.e. the limit as $h \to 0$ of the real part of a resonance), all the cases when E_0 is the common limit of two distinct h-dependent resonant energies have to be considered. In particular, the generic case and any relevant combination of the Critical case 1 can still occur. Once this is done, another case is possible when $\delta_\ell^E \le 0$ and $\delta_r^E \le 0$. The possible values of $t_1^{E_0}$ and $t_2^{E_0}$ can be restricted to the next three cases :

$$t_1^{E_0} = 1, \quad t_2^{E_0} \in [0,1]\,, \quad \text{when} \quad d_{Ag}(0,c_\ell^{E_0};\tilde{\mathcal{V}} - E_0) < d_{Ag}(c_r^{E_0},1;\tilde{\mathcal{V}} - E_0)\,, \tag{4.5}$$

$$t_1^{E_0} \in [0,1], \quad t_2^{E_0} = 0\,, \quad \text{when} \quad d_{Ag}(0,c_\ell^{E_0};\tilde{\mathcal{V}} - E_0) > d_{Ag}(c_r^{E_0},1;\tilde{\mathcal{V}} - E_0)\,, \tag{4.6}$$

$$0 \le t_2^{E_0} \le t_1^{E_0} \le 1\,, \quad \text{when} \quad d_{Ag}(0,c_\ell^{E_0};\tilde{\mathcal{V}} - E_0) = d_{Ag}(c_r^{E_0},1;\tilde{\mathcal{V}} - E_0)\,. \tag{4.7}$$

Details about this are provided in Appendix A. Cases where more than two resonant energies can meet, $\#J^E > 2$, will not be considered. In this framework, with some specific families $(V^h)_{h\in(0,h_0)}$ and with additional assumptions on the positions c_j, $j \in \{1,\dots,N\}$, it is checked in [32] and in Appendix A that all the above cases can occur and that the previous enumeration exhausts all the possibilities. We shall take this combination of possibilities for granted in our asymptotic model.

4.2 Nonlinear asymptotics.

Here are the mathematical results which were rigorously proved in [32, 33] with Hypotheses 4.1 and 4.2.

We introduce the functional spaces :

$$BV^2([0,1]) = \left\{V \in \mathcal{C}^0([0,1]) \text{ s. t. } V'' \in \mathcal{M}_b(0,1)\right\},$$

then $BV^2([0,1])$ is continuously embedded in $\mathcal{C}^{0,\alpha}(0,1)$, for any $\alpha \in (0,1)$.

$$BV_0^2([0,1])_+ = \left\{V \in BV^2([0,1]) \text{ s. t. } V \geq 0,\, V(0) = V(1) = 0\right\}.$$

By setting $c_0 = 0$ and $c_{N+1} = 1$, we introduce the set of piecewise affine functions :

$$\mathbb{P}_0^1(\mathbf{c})_+ := \left\{V \in \mathbb{P}^1(\mathbf{c}),\, V \geq 0\right\},$$

with $\mathbb{P}^1(\mathbf{c})$ the usual set of continuous $\mathbb{P}^1$ finite elements associated with the nodes $\mathbf{c} = \{c_0, c_1, \dots, c_{N+1}\}$, $c_0 = 0$, $c_{N+1} = 1$.

Theorem 4.6. *Under Hypothesis 4.1 and Hypothesis 4.2 (with g placed by $\tilde{g}$ in* (3.2)*), the solutions V_{NL}^h, $h \in (0,1]$, of the system* (3.2)

$$\left\{\begin{array}{l} -\Delta V_{NL}^h = \gamma n, \\ V_{NL}^h(0) = V_{NL}^h(1) = 0, \end{array}\right.$$

describe a bounded set of $BV_0^2([0,1])_+$. The set $\mathcal{A}$ of its limit points as $h \to 0$ is a subset of $\mathbb{P}_0^1(\mathbf{c})_+$. Moreover, any $V \in \mathcal{A}$ solves

$$-\Delta V = \sum_{E\in\mathcal{E}\cap[\Lambda_*,\Lambda^*]} \sum_{j\in J^E} t_j^E\, \tilde{g}(E)\, \delta_{c_j}, \quad V(0) = V(1) = 0, \tag{4.8}$$

where the coefficients t_j^E, satisfy

$$t_j^E \in [0,1] \quad \textit{and} \quad \left\{\begin{array}{l} \delta_\ell^E > 0 \Rightarrow t_j^E = 1,\ \forall j \in J^E, \\ \delta_r^E > 0 \Rightarrow t_j^E = 0,\ \forall j \in J^E. \end{array}\right. \tag{4.9}$$

Let $\mathcal{C}$ be the set

$$\mathcal{C} := \{V \in \mathbb{P}_0^1(\mathbf{c})_+ \text{ s. t. } \forall E \in \mathcal{E}\cap[\Lambda_*,\Lambda^*],\ (\delta_\ell^E > 0 \text{ or } \delta_r^E > 0)\}.$$

The possible limits lying in $\mathcal{C}$ can be given by a variational formulation using

$$G(E) = -\int_E^{+\infty} \tilde{g}(\lambda)\, d\lambda.$$

Corollary 4.7. *The set $\mathcal{A} \cap \mathcal{C}$ is given by the collection of critical points in $\mathbb{P}_0^1(\mathbf{c})_+$ for the functionals*

$$\mathcal{J}_{\mathcal{K}}(V) = \frac{1}{2}\int_0^1 |\partial_x V(x)|^2 \, dx - \sum_{E\in\mathcal{K}} G(E), \tag{4.10}$$

which satisfy the compatibility condition

$$\mathcal{K} = \left\{ E \in \mathcal{E} \cap [\Lambda_*, \Lambda^*] \text{ s. t. } \delta_\ell^E > 0 \right\}.$$

The previous result covers in a slightly wider generality what we called the "generic case" in the previous Subsection. It does not say anything about $\mathcal{A} \setminus \mathcal{C}$. Actually, Theorem 4.6 can be combined with the discussion of Subsection 4.1 in order to get a full description, possibly too wide, of $\mathcal{A}$. The important point is that Theorem 4.6 reduces an infinite dimensional nonlinear system which couples in a non trivial way spectral quantities with an elliptic PDE, to a collection of simple finite dimensional nonlinear systems. Further, a full description of this collection of nonlinear systems involves the comparison of some Agmon distances.

Before going further in this direction, we first present how the theoretical results have to be interpreted and adapted in order to fit with the more realistic model.

4.3 Realistic injection profile.

The Hypothesis 4.2 about the compact support of $\tilde{g}$ is a technical assumption which simplifies at different points the mathematical analysis. Of course it is not satisfied by the Fermi-Dirac distribution function g in (3.2). The two extremities $+\infty$ and 0 are analyzed on different bases.
First the Fermi-Dirac distribution function decays exponentially fast with respect to the energy like any thermodynamical equilibrium distribution function. Truncating at high energy is physically relevant and necessary for a numerical treatment. The assumption that the compact support $\mathrm{supp}\, g$ is included in $[0,\Lambda^*] \subset [0, V_0 - B)$ can be extended to $[0,\Lambda^*] \subset [0, V_0)$. It will be relevant for realistic physical data provided that the temperature T and the donor density n_D are not too high (with our dimensionless parameter $V_0 > 1$ and β large enough).
The treatment of the energy 0 has to be done with more care. Actually, it is known that the crossing of the energy 0 by the resonant energies explains the negative differential resistance or the hysteresis phenomenon. A complete rigorous mathematical approach can be performed by starting from Theorem 4.6 as follows :

0) Replace the function g in (3.2) by a function compactly supported in $[0,\Lambda^*] \subset [0, V_0)$;

1) Take a function $\chi \in \mathcal{C}^\infty(0,+\infty)$ such that $\chi \equiv 1$ on $[1,+\infty)$ and $\chi \equiv 0$ for $[0,1/2]$;

2) Set for $\varepsilon > 0$, $\tilde{g}_\varepsilon(x) = \chi(\frac{x}{\varepsilon}) g(x)$;

3) Denote by $\mathcal{V}_{NL}^{\varepsilon,h}$ the possible solutions of the system (3.2) with g replaced by $\tilde{g}_\varepsilon$;

4) Consider the two steps asymptotics as $\varepsilon \to 0$ after $h \to 0$.

According to Theorem 4.6 and for any $\varepsilon > 0$, the limit points of $V_{NL}^{\varepsilon,h}$ describe a bounded set $\mathcal{A}^\varepsilon$ of piecewise affine potentials which solve (4.8) with $\tilde{g}$ replaced by $\tilde{g}_\varepsilon$. The possible limits as $\varepsilon \to 0$ belong to the set $\mathcal{A}$ of solutions to

$$-\Delta V = \sum_{E\in\mathcal{E}\cap[0,\Lambda^*]} \sum_{j\in J^E} t_j^E \, g(E) \, \delta_{c_j}, \quad V(0) = V(1) = 0, \tag{4.11}$$

$$\text{where} \qquad g(0) \in \left[0, g(0^+)\right] \quad \text{is arbitrary,}$$

and where the coefficients t_j^E, satisfy

$$t_j^E \in [0,1] \quad \text{and} \quad \begin{cases} \delta_\ell^E > 0 & \Rightarrow \quad t_j^E = 1,\ \forall j \in J^E, \\ \delta_r^E > 0 & \Rightarrow \quad t_j^E = 0,\ \forall j \in J^E. \end{cases} \tag{4.12}$$

In connection with the variational formulation of Corollary 4.7, an interesting property related in some sense to the thermodynamical stability is due to the fact that g is a decaying function. Set

$$\dot{\mathcal{C}} := \left\{ V \in \mathbb{P}_0^1(\mathbf{c})_+ \text{ s. t. } 0 \notin \mathcal{E} \text{ and } \forall E \in \mathcal{E} \cap (0,\Lambda^*],\ (\delta_\ell^E > 0 \text{ or } \delta_r^E > 0) \right\},$$

$$\text{and} \qquad G(E) = -\int_E^{\Lambda^*} g(\lambda)\, d\lambda, \quad \text{for } E \in [0,\Lambda^*].$$

Proposition 4.8. *The set $\mathcal{A} \cap \dot{\mathcal{C}}$ is given by the collection of critical points in $\mathbb{P}_0^1(\mathbf{c})_+$ for the functionals*

$$\mathcal{J}_{\mathcal{K}}(V) = \frac{1}{2}\int_0^1 |\partial_x V(x)|^2\, dx - \sum_{E \in \mathcal{K}} G(E), \tag{4.13}$$

which satisfy the compatibility condition

$$\mathcal{K} = \left\{ E \in \mathcal{E} \cap (0,\Lambda^*] \text{ s. t. } \delta_\ell^E > 0 \right\}, \quad 0 \notin \mathcal{E}.$$

When g is decreasing on $(0,\Lambda^*)$, the functional $\mathcal{J}_{\mathcal{K}}$ is strictly convex for any fixed $\mathcal{K}$ and there exists at most one critical point.

Hence for generic cases which avoid $0 \in \mathcal{E}$, the problem is reduced to a finite collection of well-posed variational nonlinear problems in finite dimension.

4.4 Injection from the two sides.

For the sake of simplicity but also for pedagogical purpose, the mathematical analysis as well as the above presentation were done in the case where the function of the momentum $g(k)$ is supported in $\{k \geq 0\}$. This presentation makes more clear the spectral anisotropy when functions of the momentum are considered instead of functions of the energy. However in realistic diodes electrons are injected from both sides with different electro-chemical potentials. Actually this two-sided injection of electrons is easily taken into account in the modelling or in the mathematical analysis as follows.

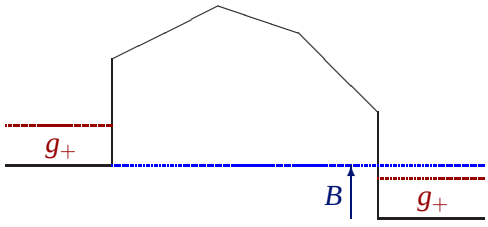

Figure 2: Injection from the two sides

Let us denote by g_+ and g_- the (truncated) Fermi-Dirac function for the injection profiles from the left and from the right respectively. When the donor density are equal in the source and in the drain, taking into account the height of the bias B provides

$$g_+(E) = g_0(E) \quad \text{and} \quad g_-(E) = g_0(E+B).$$

Since the momentum function has the form

$$g(k) = g_+(k^2)1_{\{k>0\}} + g_-(k^2 - B)1_{\{k<0\}},$$

we write

$$g(k) = \left(g_+(k^2) - g_-(k^2)\right) 1_{\{k>0\}} + \left(g_-(k^2 - B)1_{\{k<0\}} + g_-(k^2)1_{\{k>0\}}\right).$$

Using the decomposition of the incoming beam in a part coming from the left-hand side and one other coming from the right-hand side, the operator form of this identity writes

$$g_+(H^h)1_{\{K^h>0\}} + g_-(H^h)1_{\{K^h<0\}} = (g_+(H^h) - g_-(H^h))1_{\{K^h>0\}} + g_-(H^h). \tag{4.14}$$

The first part of the right-hand side of (4.14) is a function of the momentum supported in $k > 0$ and the second is a function of the energy.

Hence Theorem 4.6 and its variation of Subsection 4.3 can be adapted by replacing $g(E)$ by $g_+(E) - g_-(E)$ in (4.11) while adding a term $g_-(E)$ without any coefficient t_j^E .

The set $\mathcal{A}$ of possible limit points of solutions to (3.2) with a two-sided injection, is the set of non negative piecewise affine potentials which solve

$$-\Delta V = \sum_{E\in\mathcal{E}} \sum_{j\in J^E} \left(t_j^E\,(g_+(E) - g_-(E))\,1_{\{[0,\Lambda^*]\}}(E) + g_-(E)\,1_{[0,\Lambda^*]}(E)\right)\delta_{c_j}, \quad V(0) = V(1) = 0, \tag{4.15}$$

with the convention that $(g_+ - g_-)(0)$ can be any value in $[0, (g_+ - g_-)(0^+)]$ and where the coefficients t_j^E satisfy the property (4.12) .
Moreover the variational formulation of Proposition 4.8 can be adapted with a similar uniqueness result when g_0 is a decreasing function.

4.5 Conclusion about the theoretical analysis.

The theoretical results show that, asymptotically as $h \to 0$, the full system (3.2) reduces to a collection of well posed simple nonlinear equations. The well posedness is confirmed by the uniqueness result of Proposition 4.8 for some generic case. Another important point which appeared in the discussion of Subsection 4.1 is that, in all the degenerate cases which were considered, any new indeterminacy of the coefficients t_j^E is compensated by a new equation. Similarly the indeterminacy of $g(0)$ in (4.11) (resp. of $(g_+ - g_-)(0)$ in (4.15)) is compensated by the equation $E = 0$.

Moreover this mathematical analysis shows what are the important quantities in this nonlinear problem. Asymptotically and for any fixed case (generic or degenerate case), the unknowns are reduced to the jumps of the potential derivative $\partial_x V$:

$$\{unknowns\} = \{total\ masses\ per\ well\}\ .$$

The important parameters are :

- The dimensionless small parameter $h \to 0$: In practical situations, the parameter h is strictly positive but reasonably small in order to exhibit resonances as very stiff spectral quantities. Remind that the asymptotic analysis was carried out in a framework which keeps a finite number of resonant states in the physically relevant energy interval. This fits very well with the cases which will be presented.

- The position of the well c_j : In the mathematical analysis, the quantum wells are asymptotically pointwise concentrated. Of course, this does not hold exactly for realistic $h > 0$. These positions will be computed as averaged positions in the wells around which the electronic density concentrates.

- The bound state energies $-\varepsilon_j^k$ of the Hamiltonian $-\Delta + W_j$: After a translation by $V(c_j)$, they are equal to the real part of the resonances or to the Dirichlet eigenvalues up to some very small error (this will be checked numerically). Those energies are parameters of the asymptotic nonlinear problem. They will be computed numerically in a linear setting before being plugged into the computation of the nonlinear solutions. Actually, as we will see in Subsection 6.1, the parameters $-\varepsilon_j^k$ and c_j will be determined similarly by the same process.

- The Agmon distances : Although they are unknowns before solving the nonlinear problem, they can be viewed as parameters in the sense that the comparison of Agmon distances parametrizes all the possible cases. Actually all the possible cases are considered in a first numerical approach and the constraints on the Agmon distances are checked afterwards in order to eliminate the irrelevant cases. Note also that the fact that for $h > 0$, the wells are not pointwise concentrated has to be taken into account in the computation of the actual Agmon distances. The details are explained in Section 7.

5 Validity of the asymptotic model.

Here it is checked on some numerical examples that the asymptotics $h \to 0$ makes sense in the simulation of realistic devices. Some examples of electronic densities, numerically computed with a large number of generalized eigenfunctions, exhibit an anisotropy phenomenon which confirms the rapid variation of the asymptotic parameter t_j^E from 1 to 0 in (4.11). All those numerical observations are presented in order to show that the asymptotic model derived as the dimensionless parameter h goes to 0 makes sense in the study of realistic devices.

5.1 Generalized eigenfunctions.

In one dimension and with the potential $\mathcal{V}^h$ which is constant outside $[0,1]$, the generalized eigenfunctions are fully determined by a k-dependent non homogeneous boundary problem on $[0,1]$.
Let us first consider the case $k > 0$. The incoming generalized eigenfunction is then characterized by $\psi_-^h(k)$:

$$\left\{\begin{array}{rcll} -h^2\dfrac{d^2}{dx^2}\psi_-^h(k,x) + \mathcal{V}^h\psi_-^h(k,x) &=& k^2\psi_-^h(k,x)\,, & \\ h\psi_-^{h\,\prime}(k,0) + ik\psi_-^h(k,0) &=& 2ik, & k>0 \\ h\psi_-^{h\,\prime}(k,1) - i\sqrt{k^2+B}\psi_-^h(k,1) &=& 0. & \end{array}\right. \tag{5.1}$$

In the case $k < 0, k^2 \neq B$, with the convention $(k^2-B)^{1/2} = i\sqrt{B-k^2}$ when $B > k^2$ (more generally $(\rho\,e^{i\theta})^{1/2} = \sqrt{\rho}\,e^{i\theta/2}$ for $\rho > 0$ and $\theta \in [0, 2\pi)$), the generalized eigenfunction $\psi_-^h(k)$ is given by

$$\left\{\begin{array}{rcll} -h^2\dfrac{d^2}{dx^2}\psi_-^h(k,x) + \mathcal{V}^h\psi_-^h(k,x) &=& (k^2-B)\psi_-^h(k,x)\,, & \\ h\psi_-^{h\,\prime}(k,0) + i(k^2-B)^{1/2}\psi_-^h(k,0) &=& 0, & k<0 \\ h\psi_-^{h\,\prime}(k,1) + ik\psi_-^h(k,1) &=& 2ik\,e^{ik/h}. & \end{array}\right. \tag{5.2}$$

Numerically, those boundary value problems are simply computed by a finite difference method. The discretization step $\Delta_x = 1/N_x$ is a parameter of the numerical method. The computation of integrated quantities with respect to k also requires a discretization in the k variable. The step Δ_k has to be chosen small enough in order to catch the resonances which produce very stiff spectral quantities when $h > 0$ is small. Actually, it is known (see for example [19, 20, 38]) that this slope is of order $e^{C/h}$. The stiffness of this spectral quantities is a first test to check that the asymptotic model for $h \to 0$ is relevant. One may question about the numerical complexity related to the choice of a very small $\Delta_k = \Lambda^*/N_k$. Actually, such calculations are done only once in the beginning in order to guess the parameters $-\varepsilon_j^k$ (and c_j, see Subsection 6.1) and in the end in the computation of the current density (see Subsection 6.2). Once those parameters are fixed, solving the asymptotic nonlinear problem (4.11) does not involve anymore the generalized eigenfunctions. Hence the numerical complexity of the accurate computations of the generalized eigenfunction is not a big issue here. For the alternative efficient numerical methods related to such problems and which deal with the generalized eigenfunctions on the ground of a WKB analysis, we quote the works of Ben Abdallah and Pinaud [7, 34, 35].

5.2 Detection of resonances.

After computing the generalized eigenfunctions by a finite difference method, we compute the local density of states with respect to the energy in each well. The stiff picks of this density of states are identified as resonances according to the Breit-Wigner formula (see [15, 32, 38]). Note that for $h > 0$, the wells are not reduced to single points. We define for each well around c_j, the function

$$M_j(E) = \int_{[c_j^-, c_j^+]} \left(|\psi_-^h(\sqrt{E}, x)|^2 + |\psi_-^h(-\sqrt{E+B}, x)|^2 \right) dx.$$

The neighbourhood $[c_j^-, c_j^+]$ of the center of the well c_j is specified further in Section 7.
Figure 3 shows the function $M_1(E)$ in a fixed well for two values $B = 0 = B_{\min}$ and $B = B_{\max}$ of the bias. It corresponds to the physically realistic case with one well presented in Subsection 9.2, case 1. We simply show the results in terms of dimensionless quantities. The errorbar on the Energy axis represents

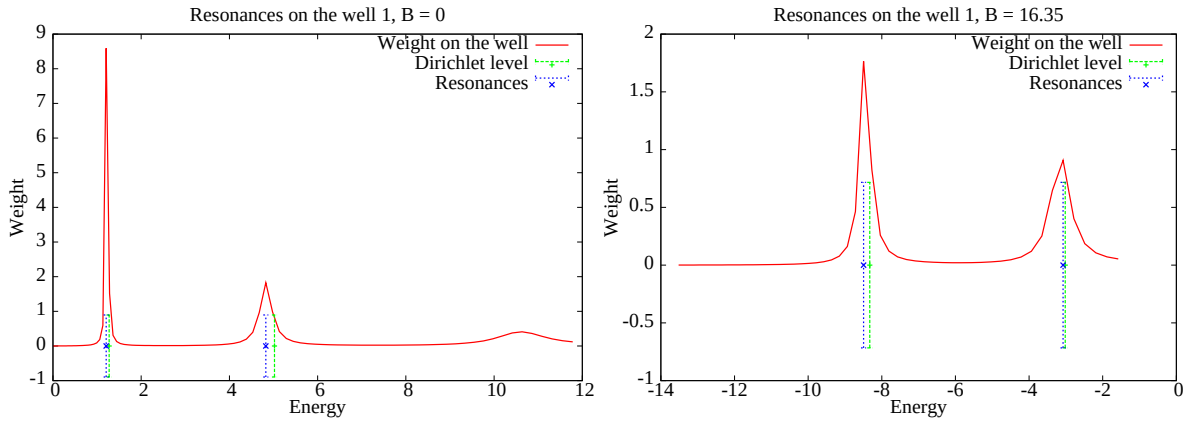

Figure 3: Determination of resonant energies

the detected resonances and the Dirichlet eigenvalues (with boundary conditions $\psi(0) = \psi(1) = 0$ instead of transparent boundary conditions in (5.2)). The very stiff picks as well as the proximity of the detected resonances and the Dirichlet eigenvalues confirms the validity of an asymptotic treatment as $h \to 0$.

5.3 Filled and empty wells for functions of the momentum.

On the ground of numerical examples, we now show that the asymptotic behaviour described in (4.9) makes sense even when $h > 0$ is not very small and lies in the range of parameters occurring in realistic configurations. We simply consider here two asymmetric barrier profiles which are related to the examples of Subsection 9.2.
The bias is 0 as well as the nonlinear potential. Instead of changing the potential, we consider the two injection profiles

$$\begin{aligned} \text{injection from the left :} \quad & g(k) = (1-k^2)_+ 1_{[0,+\infty)}(k), \\ \text{injection from the right :} \quad & g(k) = (1-k^2)_+ 1_{(-\infty,0]}(k). \end{aligned}$$

Let us first analyze the device described on Figure 4. For this device with one well, we have $h = 0.17$. The size of the barriers are respectively 0.5 nm and 0.8 nm and the width of the well is 4 nm. With

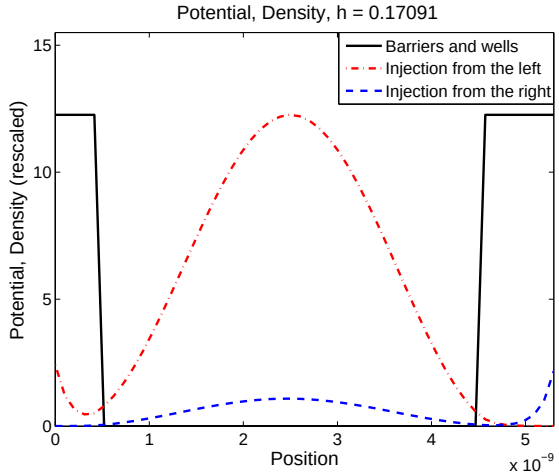

Figure 4: Effect of injection from the left or from the right.

electrons coming from the left-hand side, then the well c is filled. This illustrates the case $t_1 = 1$ in (4.9). With electrons coming from the right-hand side, then the well c is not filled. This illustrates the case $t_1 = 0$ in (4.9). Note that $h = 0.17$ is not very small and that the width of the barriers does not show a big asymmetry. This example is investigated in Subsection 9.2, case 1. Here, the size of the barriers and the wells have been changed a little in order to emphasize the Agmon distance effects.
Actually in examples associated with AsGa devices, the transition from $t_1 = 1$ to $t_1 = 0$ is even more sensitive to the variation of the widths of the barriers.

Figure 5 shows a device with two wells. The widths of barriers are respectively 0.5, 0.5 and 0.6 nm and the widths of the wells are 1.5 and 1 nm. In this device, we have $h = 0.13$ and there is one resonant states per well, with resonant energies $\mathcal{E} = \{E_1, E_2\}$. The corresponding Agmon distance satisfy

$$d_{\mathrm{Ag}}(0, c_1; \mathcal{V} - E_1) < d_{\mathrm{Ag}}(c_1, 1; \mathcal{V} - E_1) \quad \text{and} \quad d_{\mathrm{Ag}}(0, c_2; \mathcal{V} - E_2) > d_{\mathrm{Ag}}(c_2, 1; \mathcal{V} - E_2).$$

If the electrons come only from the left, then (4.9) gives $t_1 = 1$ and $t_2 = 0$, in agreement with the

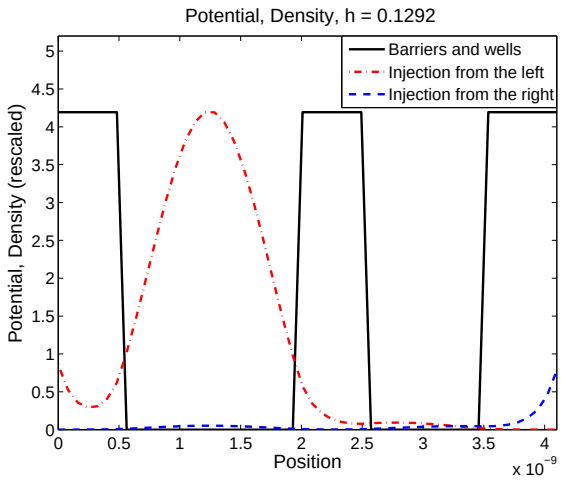

Figure 5: Effect of injection from the left or from the right on a device with two wells.

numerical results. On the other hand, with injection from the right, no well is filled since the resonant energy E_2 in the second well is too high.
We will come back to this example in Subsection 9.2, case 4.

5.4 Piecewise affine potential.

Restricting the nonlinear potential to the class of piecewise affine potential is the key point which permits to reduce the complexity of the full nonlinear system (3.2), in the limit $h \to 0$. It is a consequence of the scaling of the wells $W_j\left(\frac{x-c_j}{h}\right)$ as quantum wells in a semiclassical island, for which the classically permitted region is asymptotically reduced to a single point. Nevertheless in practical cases, h is not 0 although reasonably small (according to the discussion of Subsection 5.2), and the wells have the same order of size as the barriers. Hopefully, the nonlinearity is not very strong because the size of a well has the same order of magnitude of the Bohr radius a_B : the effective nonlinearity in the j-th well is of order $\gamma_j = \frac{4L_j}{a_B}$ after adapting the scaling (3.4) to a single well. Therefore the difference between the true nonlinear potential and its piecewise affine approximation can be neglected when the position c_j is chosen close to the center of mass of the electron density in the j-th well according to the next picture 6.

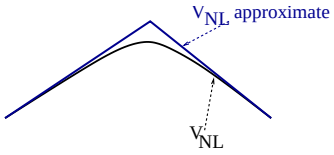

Figure 6: Approximation of the nonlinear potential.

The exactly used value of the position c_j is presented in the Subsection 6.1.

6 Implementation of the asymptotic model.

Here we show how the asymptotic model derived after taking the limit $h \to 0$ in Section 4 is adapted to physically relevant geometries, $h > 0$.

6.1 Position of the wells c_j and resonant depths ε_j^k.

Here we explain how the parameters c_j and ε_j^k, $k = 1, \dots, K_j$ are determined in realistic $h > 0$ cases. With those parameters, the k-th resonant energy level attached to the j-th well is given in the asymptotic model by

$$E_j^k = \tilde{\mathcal{V}}(c_j) - \varepsilon_j^k, \tag{6.1}$$

according to (4.1)–(4.2). Actually we restrict first our attention to the case $K_j = 1$ and write simply ε_j instead of ε_j^1. Fortunately the process that we describe in this simpler case admits a natural and easily implementable extension to $K_j > 1$ by accepting several values c_j^k of the center of mass of the well. Details are given about this in the end of this paragraph and in Section 7.

The determination of c_j and ε_j is done simultaneously without requiring additional heavy numerical computation. It is a linear interpolation process which relies on the following heuristic.

An intermediate step to show that the resonant energy in the j-th well is close to $\tilde{\mathcal{V}}(c_j) - \varepsilon_j$ relies on the fact that it is at a distance $\tilde{O}(e^{-c/h})$ from some eigenvalue of (5.1), with the energy-dependent absorbing boundary conditions replaced by homogeneous Dirichlet boundary conditions. Hence one can work with those Dirichlet eigenvalues of which the eigenfunctions are localized in the quantum wells. Those Dirichlet eigenvalues admit a first order perturbation according to the Feynmann-Hellman law

$$\delta E = \langle \psi | \delta V \psi \rangle ,$$

when ψ is a normalized eigenfunction at energy E, δV is the variation of the Hamiltonian and δE the corresponding variation of the eigenvalue. Moreover when $\delta V = \delta V(\nu x)$, with $\nu > 0$ small, varies on a slower scale than ψ, a second order Taylor expansion of $\delta V(c + \nu(x-c))$ leads to

$$\langle \psi | \delta V \psi \rangle = \int \delta V(\nu x) \, |\psi(x)|^2 \, dx = \delta V(c) + O(\nu^2) ,$$

where c is the center of mass of the probability density $|\psi|^2$:

$$\int (x-c) \, |\psi(x)|^2 \, dx = 0 .$$

The resonant energies associated with each well can be determined according to the process described in Subsection 5.2. These computations are done for the two extreme values of the applied bias, B_{min} and B_{max}, and with no nonlinear potential ($V_{NL}^h \equiv 0$). This provides in the well j the two resonant energies $E_j(B_{min})$ and $E_j(B_{max})$. The variation of the potential by changing the bias is the affine function $\delta V(x) = -(B_{max} - B_{min})x$ for $x \in [0,1]$. The previous discussion says that the center of mass c_j can be approximated according to

$$E_j(B_{max}) - E_j(B_{min}) = -(B_{max} - B_{min}) c_j . \tag{6.2}$$

Finally the approximation $E_j \sim \tilde{\mathcal{V}}(c_j) - \varepsilon_j$ provides the value ε_j by using

$$E_j(B) = V_0 - B c_j - \varepsilon_j , \tag{6.3}$$

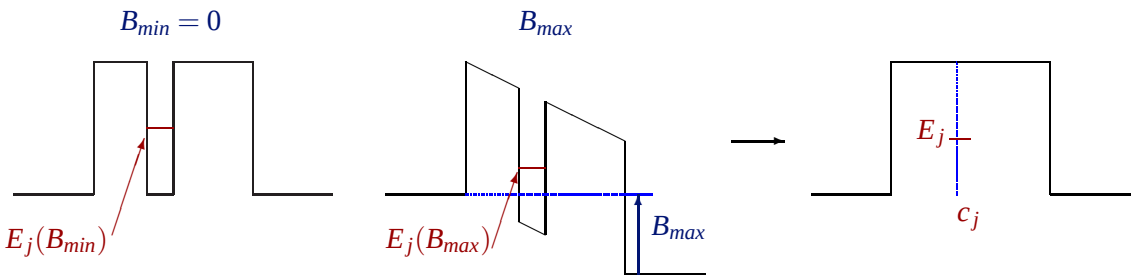

Figure 7: Determination of the resonant depth ε_j and of the averaged position c_j of the j-th well.

applied with $B = B_{max}$ or $B = B_{min}$ (both are compatible according to (6.2)).

Figure 7 summarizes how the parameters (c_j, ε_j) (occurring in the asymptotic model $h \to 0$) are fitted to the numerical values of resonant energies ($h > 0$). Figure 8 shows in a practical case the actual density and the position c_j of the simplifying delta function. We end this paragraph with two remarks.

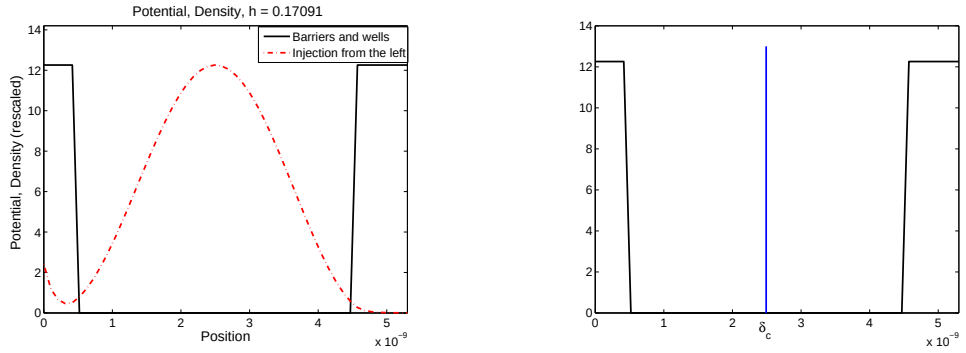

Figure 8: Density on the well and position of the asymptotics well.

Remark 6.1. ***1)*** *The case of Figure 8 seems at a first glance to be far from the situation of (narrow) quantum wells in a semiclassical island (wide barriers). Actually the barriers can be considered as wide enough when they lead to a stiff localization of the resonant energies (see Subsection 5.2). Meanwhile replacing the real electronic density by a delta function will not bring a big error when the width of the well is less than the Bohr radius a_B.*
2) *We focused on the case when there is one single resonant state per well. A simple way to introduce several resonant energies E_j^k, $1 \le k \le K_j$, per well can be done by determining several averaged positions according to (6.2), c_j^k, $1 \le k \le K_j$. This can also be interpreted as K_j wells separated by barriers with vanishing widths (cf. Figure 11).*

6.2 Current density.

Another drawback of the asymptotic model obtained as $h \to 0$ is that the current density J defined in Subsection 3.7 vanishes as $h \to 0$. In the current-voltage characteristic curves which are presented here, the current density is computed for $h > 0$ with the help of the generalized eigenfunctions, once the nonlinear potential is computed with the asymptotic model. Hence the computation of the generalized

eigenfunction which presents the highest complexity is done first to determine the parameters (c_j, ε_j) of the asymptotic nonlinear problem and in the end in order to compute the current density.

7 Computation of Agmon distances for a piecewise affine potential.

After Subsection 5.4, the nonlinear potential V_{NL}^h can be replaced by the piecewise affine asymptotic potential V of Theorem 4.6. Then the Agmon distances, which are involved in the definition of the different cases, admit an explicit algebraic expression which is specified here. Since small variations of the Agmon distances have a strong effect on the nonlinear problem, it is better here to compute these quantities with the real size of the wells and barriers. The left-hand side of Figure 9 illustrates the asymptotics model with a total potential $\tilde{\mathcal{V}}$, which is piecewise affine, while the right-hand side presents a physically realistic case, with non vanishing well widths, for which the potential is denoted $\mathcal{V} = \tilde{\mathcal{V}} + W$, with $-V_0 \leq W \leq 0$.

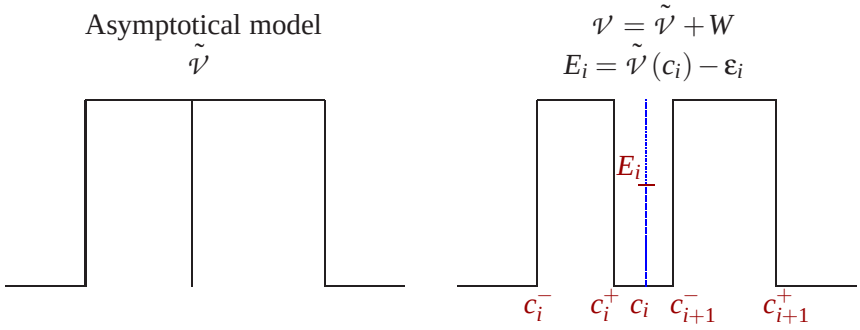

Figure 9: Determination of the points characterizing a well

With the point c_i, the left and right ends of the barrier before c_i are denoted by c_i^- and c_i^+. For an energy $E \geq \max\{\mathcal{V}(x),\ x \in [c_i^+, c_{i+1}^-]\}$, the Agmon distances satisfy the relationship :

$$d_{Ag}(c_i^-, c_i; \mathcal{V} - E) = d_{Ag}(c_i^-, c_i^+; \tilde{\mathcal{V}} - E),$$
$$\text{and} \quad d_{Ag}(c_i, c_{i+1}^+; \mathcal{V} - E) = d_{Ag}(c_{i+1}^-, c_{i+1}^+; \tilde{\mathcal{V}} - E).$$

According to (6.1) and by considering only the case $K_i = 1$ according to Remark 6.1, the resonant energy attached to the well i equals :

$$E_i = \tilde{\mathcal{V}}(c_i) - \varepsilon_i.$$

In agreement with all our numerical experiments, the non negative resonant energies are assumed to lie above the bottom of the wells : $E_i \geq \max\{\mathcal{V}(x), \quad x \in [c_k^+, c_{k+1}^-],\ 1 \leq k \leq N\}$ when $E_i \geq 0$. Then, the Agmon distances which are involved in the weight t_i, attached to the non negative resonant energy $E_i \geq 0$, are given by

$$\begin{aligned} d_{-,i} &= d_{Ag}(0, c_i; \mathcal{V} - E_i) \\ &= \sum_{k=1}^{i} d_{Ag}(c_{k-1}, c_k; \mathcal{V} - E_i) = \sum_{k=1}^{i} d_{Ag}(c_k^-, c_k^+; \tilde{\mathcal{V}} - E_i), \qquad (7.1) \\ \text{and} \quad d_{+,i} &= d_{Ag}(c_i, 1; \mathcal{V} - E_i) \\ &= \sum_{k=i+1}^{N+1} d_{Ag}(c_{k-1}, c_k; \mathcal{V} - E_i) = \sum_{k=i+1}^{N+1} d_{Ag}(c_k^-, c_k^+; \tilde{\mathcal{V}} - E_i), \qquad (7.2) \end{aligned}$$

with $c_0 = 0$ and $c_{N+1} = 1$. It remains to compute each term, $d_{Ag}(c_k^-, c_k^+; \tilde{\mathcal{V}} - E_i)$. It is convenient to introduce the quantity

$$y_{k,i}^{\pm} = \frac{\tilde{\mathcal{V}}(c_k^{\pm}) - \tilde{\mathcal{V}}(c_i)}{\varepsilon_i},$$

which permits to simplify the expression of $d_{Ag}(c_k^-, c_k^+; \tilde{\mathcal{V}} - E_i)$ and to write

$$y_{k,i}^{\pm} \geq -1 \quad \Longleftrightarrow \quad E_i = \tilde{\mathcal{V}}(c_i) - \varepsilon_i \leq \tilde{\mathcal{V}}(c_k^{\pm}).$$

Several cases have to be considered (cf. Figure 11) :

First case : $E_i \leq \tilde{\mathcal{V}}(c_k^-)$ and $E_i \leq \tilde{\mathcal{V}}(c_k^+)$. A simple integration gives

$$\begin{aligned} d_{Ag}(c_k^-, c_k^+; \tilde{\mathcal{V}} - E_i) &= \int_{c_k^-}^{c_k^+} \sqrt{\tilde{\mathcal{V}}(x) - \tilde{\mathcal{V}}(c_i) + \varepsilon_i}\, dx \\ &= \frac{2}{3}\sqrt{\varepsilon_i}(c_k^+ - c_k^-)\frac{(y_{k,i}^+ + 1)^{3/2} - (y_{k,i}^- + 1)^{3/2}}{y_{k,i}^+ - y_{k,i}^-}, \end{aligned}$$

with $y_{k,i}^{\pm} \geq -1$.

Second case : $E_i \leq \tilde{\mathcal{V}}(c_k^-)$ and $E_i \geq \tilde{\mathcal{V}}(c_k^+)$.

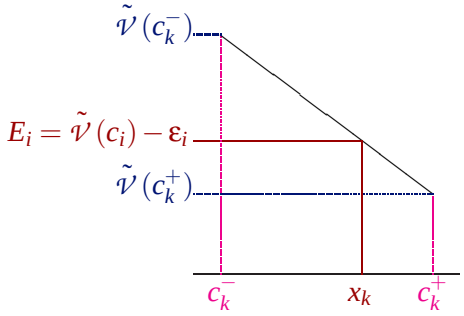

Figure 10: Configuration of the second case

As illustrated in Figure 10, the intersection point $x_k \in [c_k^-, c_k^+]$ such that $\tilde{\mathcal{V}}(x_k) = E_i = \tilde{\mathcal{V}}(c_i) - \varepsilon_i$ is given by

$$\frac{x_k - c_k^-}{c_k^+ - c_k^-} = \frac{\tilde{\mathcal{V}}(c_k^-) - \tilde{\mathcal{V}}(c_i) + \varepsilon_i}{\tilde{\mathcal{V}}(c_k^-) - \tilde{\mathcal{V}}(c_k^+)}.$$

This leads to

$$\begin{aligned} d_{Ag}(c_k^-, c_k^+; \tilde{\mathcal{V}} - E_i) &= d_{Ag}(c_k^-, x_k; \tilde{\mathcal{V}} - E_i) \\ &= \int_{c_k^-}^{x_k} \sqrt{\tilde{\mathcal{V}}(x) - \tilde{\mathcal{V}}(c_i) + \varepsilon_i}\, dx = -\frac{2}{3}\sqrt{\varepsilon_i}(c_k^+ - c_k^-)\frac{(y_{k,i}^- + 1)^{3/2}}{y_{k,i}^+ - y_{k,i}^-}. \end{aligned}$$

All the other cases amount to these two ones.
This leads to the expressions

$$d_{i,-} = \frac{2}{3}\sqrt{\varepsilon_i}\sum_{k=1}^{i}(c_k^+ - c_k^-)\,f(y_k^+, y_k^-)\,, \tag{7.3}$$

$$d_{+,i} = \frac{2}{3}\sqrt{\varepsilon_i}\sum_{k=i+1}^{N+1}(c_k^+ - c_k^-)\,f(y_k^+, y_k^-)\,, \tag{7.4}$$

where the symmetric function f is given by

$$f(y_1,y_2) = \begin{cases} \dfrac{(y_1+1)^{3/2}-(y_2+1)^{3/2}}{y_1-y_2} & \text{if } y_1 \geq -1,\ y_2 \geq -1 \text{ and } y_1 \neq y_2\,, \\ \dfrac{3}{2}\sqrt{y_1+1} & \text{if } y_1 \geq -1,\ y_2 \geq -1 \text{ and } y_1 = y_2+\varepsilon\,, \\ -\dfrac{(y_2+1)^{3/2}}{y_1-y_2} & \text{if } y_1 \leq -1 \text{ and } y_2 \geq -1\,, \\ \dfrac{(y_1+1)^{3/2}}{y_1-y_2} & \text{if } y_1 \geq -1 \text{ and } y_2 \leq -1\,, \\ 0 & \text{else.} \end{cases}$$

The Newton algorithms used in solving numerically the nonlinear problem also requires the expressions of the derivatives of (7.3)–(7.4). By setting $V_j = \tilde{\mathcal{V}}(c_j)$, the definition of $y_{k,i}^{\pm}$ leads to

$$\frac{\partial d_{Ag}(c_k^-, c_k^+; \tilde{\mathcal{V}} - E_i)}{\partial V_j} = \frac{2}{3}\frac{(c_k - c_{k-1})(r_k^+ - r_k^-)}{\sqrt{E_i}}\Big[\left((1-r_k^+)\partial_1 f(y_k^+, y_k^-) + (1-r_k^-)\partial_1 f(y_k^-, y_k^+)\right)\,\delta_{k,j+1} + \left(r_k^+\partial_1 f(y_k^+, y_k^-) + r_k^-\partial_1 f(y_k^-, y_k^+)\right)\,\delta_{k,j} - \left(\partial_1 f(y_k^+, y_k^-) + \partial_1 f(y_k^-, y_k^+)\right)\delta_{i,j}\Big]\,,$$

with $r_k^{\pm} = \dfrac{c_k^{\pm} - c_{k-1}}{c_k - c_{k-1}}$, for any $i, j \in \{1,\ldots,N\}$ and any $k \in \{1,\ldots,N+1\}$. The derivative $\partial_1 f$ equals

$$\partial_1 f(y_1,y_2) = \begin{cases} \dfrac{\frac{3}{2}(y_1+1)^{1/2}(y_1-y_2) - (y_1+1)^{3/2} + (y_2+1)^{3/2}}{(y_1-y_2)^2} & \text{if } y_1 \geq -1,\ y_2 \geq -1 \text{ and } y_1 \neq y_2, \\ \dfrac{3}{8}\dfrac{1}{\sqrt{y_1+1}} & \text{if } y_1 \geq -1,\ y_2 \geq -1 \text{ and } y_1 = y_2, \\ \dfrac{(y_2+1)^{3/2}}{(y_1-y_2)^2} & \text{if } y_1 \leq -1 \text{ and } y_2 \geq -1, \\ \dfrac{\frac{3}{2}(y_1+1)^{1/2}(y_1-y_2) - (y_1+1)^{3/2}}{(y_1-y_2)^2} & \text{if } y_1 \geq -1 \text{ and } y_2 \leq -1, \\ 0 & \text{else.} \end{cases}$$

The derivatives $\partial_{V_j} d_{\pm,i}$ are obtained by summing over $k \in \{1,\ldots,i\}$ or $k \in \{i+1,\ldots,N+1\}$.

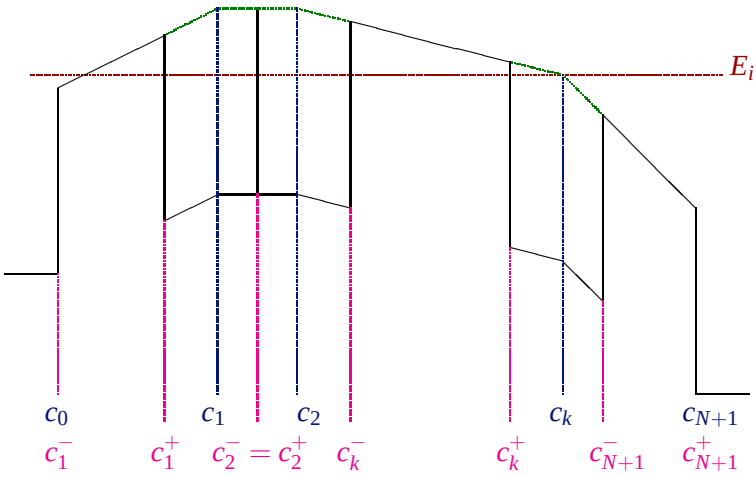

Figure 11: Notation for a device

8 Penalization method.

The constraints which involve the Agmon distance in Theorem 4.6 have no obvious convexity properties. The simplest and robust way to take them into account is a penalization method. We set $t_j = \tau_j \theta_j$ with

$$\theta_j = \frac{1}{1+\exp\dfrac{d_{\mathrm{Ag}}(0,c_j;\mathcal{V}-E_j) - d_{\mathrm{Ag}}(c_j,1;\mathcal{V}-E_j)}{\varepsilon}},$$

and for any resonances, we distinguish three cases :

$$\begin{aligned} E_j = \tilde{\mathcal{V}}(c_j) - \varepsilon_j > 0, &\qquad \tau_j = 1, \\ E_j = \tilde{\mathcal{V}}(c_j) - \varepsilon_j < 0, &\qquad \tau_j = 0, \\ E_j = \tilde{\mathcal{V}}(c_j) - \varepsilon_j = 0, &\quad \tau_j \in (0,1). \end{aligned}$$

The penalization parameter $\varepsilon > 0$ has to be small enough in order to have a realistic treatment of the constraint but not too small in order to keep a well-behaved Newton algorithm. In the original problem, the Agmon distances occur in factors which behave like $e^{\frac{d_{\mathrm{Ag}}(0,c_j;\mathcal{V}-E_j) - d_{\mathrm{Ag}}(c_j,1;\mathcal{V}-E_j)}{h}}$. Therefore, values between $\varepsilon = 0$ and $\varepsilon = h$ make sense. The two extreme cases $\varepsilon = 0$ and $\varepsilon = h$ have been tested. The possibility to take $\varepsilon = \mathcal{O}(h)$ implements a soft transition between $\theta_j = 0$ and $\theta_j = 1$ as it may occur when h is not very small.

The algorithm relies on a continuation for the 3^N cases corresponding to the three possible values of τ_j and the N wells. The critical case coming from the equality of the Agmon distance (only) in the case with 2 wells, is treated separatly.
The conditions $\tau_j \in [0,1]$, $E_j > 0$, $E_j < 0$ are verified *a posteriori*.

9 Numerical results.

In this Section, we show how our numerical approach is flexible and seems to catch in a very efficient way the main quantities involved in the nonlinear problem. These computations were realized on a laptop

with a Gnu Octave program (similar to MATLAB). The indicated "CPU time" refers to the CPU time in seconds used to solve the non linear problem without computing the current. The time used for this last part varies from one case to the other and can be significantly longer. The core of the program which is the rapid one permits to get very quickly an idea of the bifurcation diagram.

9.1 Computations for GaAs.

We consider data of O. Pinaud proposed in [34, 35]. Let us recall some physical parameters :

Relative mass	0.067	h	0.22
Relative permitivity	11.4	$B_{\min}$	0 eV
Temperature	300 K	$B_{\max}$	0.25 eV
Donor density	10^{24} m^{-3}	Height of barriers	0.3 eV
Fermi level E_F	0.054 eV		

9.1.1 Case 1.

Let us consider firstly a device with one well and two barriers at equal size. The characteristic of this device and the parameter of experiment are the following :

Size of barriers	$50\ 10^{-10}$, $50\ 10^{-10}$ m
Size of well	$50\ 10^{-10}$ m
Penalization parameter	$\varepsilon = 0.001$
Discretization in voltage	100 points
Discretization in energy	1000 points
Position of the well	$c_1 = 78\ 10^{-10}$ m
Resonance depth	$\varepsilon_1 = 0.21$ eV
CPU time	9.21

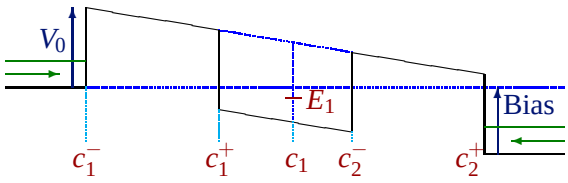

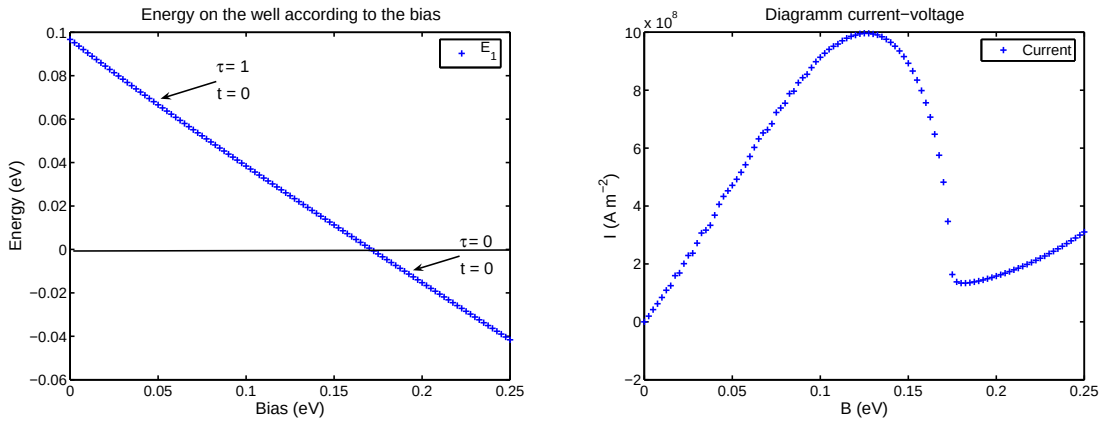

Figure 12: Negative differential resistance

We notice that there is no hysteresis phenomenon. The approximation of the current needs a fine discretization in energy. Those results are close to those of O. Pinaud (see [34]) : For the same configuration, we obtain a similar magnitude for the current and the negative differential resistance occurs for the same place.

9.1.2 Case 2.

We now consider a new device for which we observe a hysteresis phenomenon.

Size of barriers	$30\ 10^{-10}$, $60\ 10^{-10}$ m
Size of well	$60\ 10^{-10}$ m
Penalization parameter	$\varepsilon = 0.01$
Discretization in voltage	100 points
Discretization in energy	200 points
Position of the well	$c_1 = 63\ 10^{-10}$ m
Resonance depth	$\varepsilon_1 = 0.227$ eV
CPU time	9.92

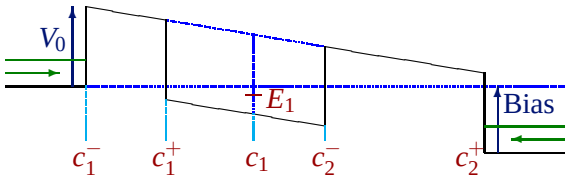

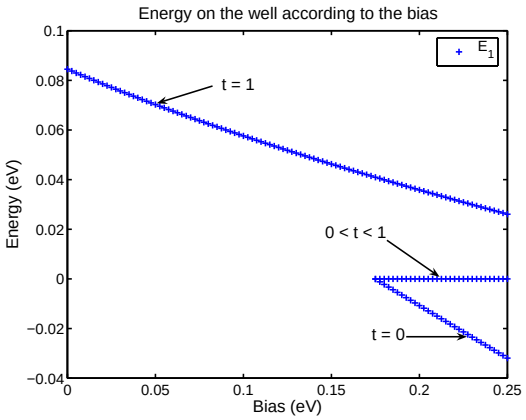

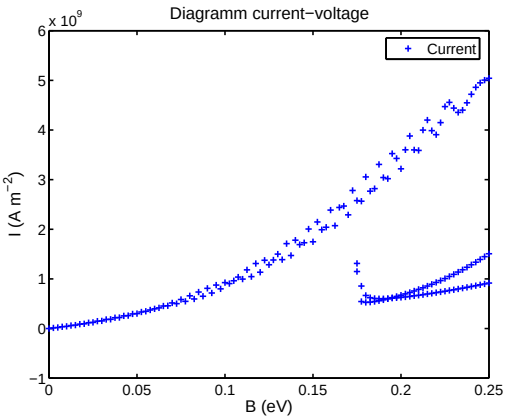

Figure 13: Hysteresis phenomenum

The hysteresis curve is not complete here. Actually, after trying several configurations, obtaining a complete hysteresis phenomenon appeared rather difficult in a GaAs-AlGaAs heterostructures.

9.2 Computations for Si.

9.2.1 Case 1.

We now consider a device in Si-SiO, whose characteristics were taken in [26]. The physical parameters are given by

Relative mass	$(0.19, 0.92, 0.19)$	Donor density	10^{26} m^{-3}
Relative permitivity	11.9	Fermi level E_F	0.245 eV
Temperature	300 K		

In this example where the two barriers have the same size, several values of the penalization parameter were tested according to the discussion of Section 8 and led here to interesting variations. Figure 14 was obtained with a smaller parameter $\varepsilon = 0.01$ while Figure 15 shows the results for $\varepsilon = h \sim 0.3$. The common characteristics between these two numerical experiments are :

$B_{\min}$	0 eV
$B_{\max}$	4 eV
Height of barrier	3 eV
Size of barriers	$5\ 10^{-10}$, $5\ 10^{-10}$ m
Size of well	$20\ 10^{-10}$ m
h	0.301933
Discretization in voltage	100 points
Discretization in energy	200 points
Position of the wells	$c_1 = 14.6\ 10^{-10}$, $c_2 = 17.7\ 10^{-10}$ m
Resonance depth	$(\varepsilon_1, \varepsilon_2) = (1.8, 2.7)$ eV

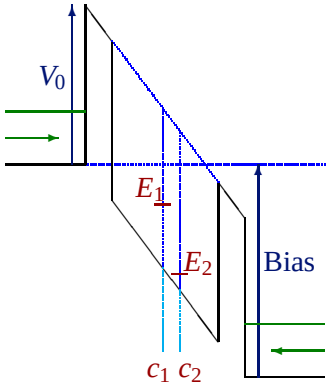

If the penalization parameter is small, $\varepsilon = 0.01$, then no hysteresis phenomenon appears as shown in Figure 14 (CPU time is equal to 38.2). The resonant energies vary linearly and only the negative differential resitance remains on the I-V diagram of Figure 14.

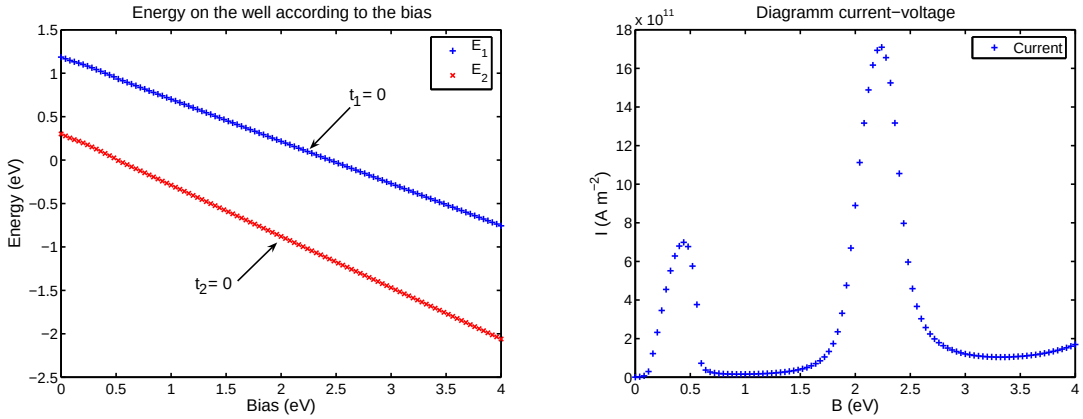

Figure 14: Small penalization parameter

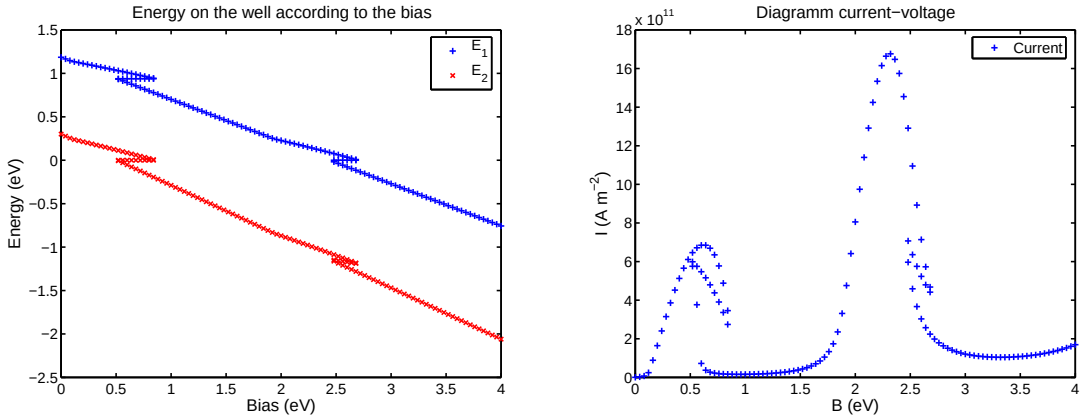

Figure 15: Penalization parameter of size h

The second choice of the penalization parameter, $\varepsilon = h = 0.301933$, shows in Figure 15 a small double hysteresis phenomenon for biases in agreement with the ones obtained in [26] (the CPU time was 54.57).

Actually the sensitivity to the penalization parameter is due to the fact that this case with two equal barriers, shows rather small differences between the right and left Agmon distances. Practically this would mean that the hysteresis phenomenon (or its absence) is rather unstable with respect to small variations of the data. As this is shown below, and as other numerical experiments in [31] showed, the hysteresis phenomenon can be strengthened when the second barrier is wider than the first one. On the contrary, it disappears as the width of the second barrier becomes significantly smaller than the first one. The choice of a penalization parameter close to $h > 0$ broadens this transition.

9.2.2 Case 2.

We now consider the device characterized by :

Donor density	10^{26} m^{-3}
Fermi level E_F	0.245 eV
$B_{\min}$	0 eV
$B_{\max}$	3 eV
Height of barrier	3 eV
Size of barriers	5 10^{-10}, 10 10^{-10} m
Size of well	25 10^{-10} m
h	0.22
Penalization parameter	$\varepsilon = 0.01$
Discretization in voltage	100 points
Discretization in energy	200 points
Position of the well	$c_1 = 17\ 10^{-10}$, $c_2 = 21\ 10^{-10}$ m
Resonance depth	$(\varepsilon_1, \varepsilon_2) = (2.2, 2.8)$ eV
CPU time	45.50

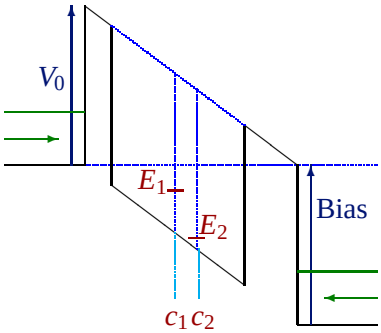

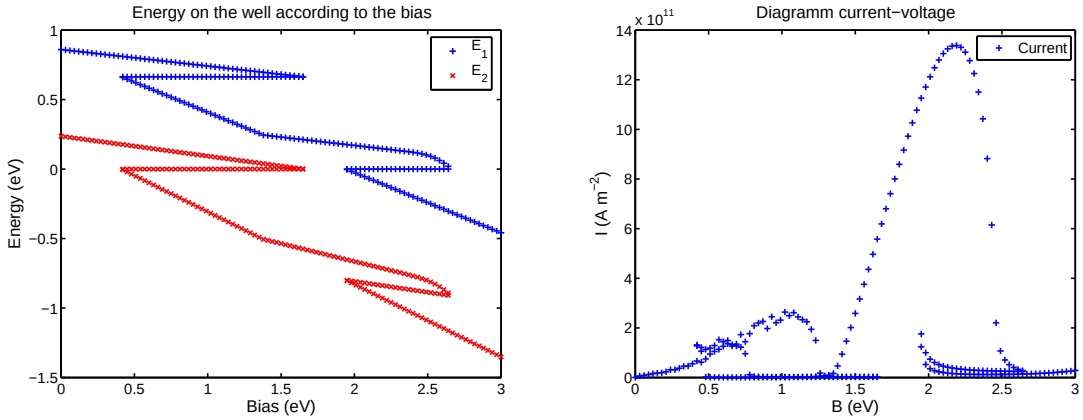

Figure 16: Hysteresis

The hysteresis appears more easily with the silicium heterostructures than with the As-Ga ones and it is more intensive, as it appears in Figure 16. In comparison with the first silicium device, the width of

the second barrier and of the well have been increased.

9.2.3 Case 3.

The very high barrier potentials permit to create cases with a double well were the two (asymptotic) resonant energies eventually take the same value. Let us consider a device with the following parameters :

Donor density	10^{26} m^{-3}
Fermi level E_F	0.245 eV
$B_{\min}$	0 eV
$B_{\max}$	2.5 eV
Height of barrier	3 eV
Size of barriers	$5\ 10^{-10}$, $5\ 10^{-10}$, $10\ 10^{-10}$ m
Size of well	$15\ 10^{-10}$, $10\ 10^{-10}$ m
h	0.2
Penalization parameter	$\varepsilon = 0.01$
Discretization in voltage	100 points
Discretization in energy	200 points
Position of the well	$c_1 = 12\ 10^{-10}$, $c_2 = 30\ 10^{-10}$ m
Resonance depth	$(\varepsilon_1, \varepsilon_2) = (2.5, 2.1)$ eV
CPU time	42.45

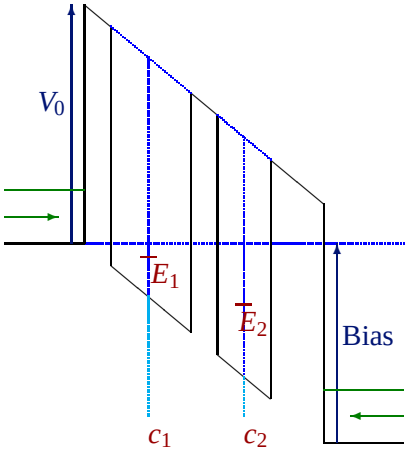

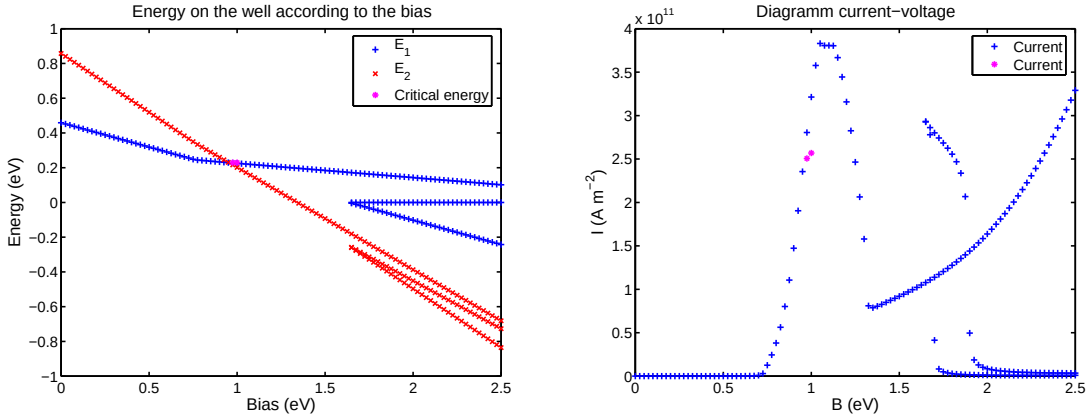

Figure 17: Crossing and Hysteresis

The second resonant energy decreases faster than the first one. They reach the same value for the bias $B \sim 1\,\text{eV}$ and a new bifurcation branch seems to develop. This last point is even more obvious in the next case.

Note that there is small piece of hysteresis phenomenon for a high applied voltage. It is coupled with an apparently strange behaviour of the current density, for $1.7\,\text{eV} \leq B \leq 2\,\text{eV}$. Actually it is an artefact of our approach : the nonlinear potential is essentially determined via the asymptotic model while the current is computed with the full linear Schrödinger system once the potential is known. The bias for which the resonant energy crosses the value 0 is not exactly detected with the asymptotic model. This generates a substancial error on the current density at this moment.

9.2.4 Case 4.

We now consider a case similar to Case 3, with a donor density equal to 5×10^{26} m^{-3}.
With two wells and according to the discussion of [31, 32, 33] summarized in Subsection 4.1, some critical cases are possible depending on the comparison of the two extreme Agmon distances. This is produced in the next example in which the first and third barrier have almost the same size.

Donor density	$5\ 10^{26}$ m^{-3}
Fermi level E_F	0.716 eV
$B_{\min}$	0 eV
$B_{\max}$	2.5 eV
Height of barrier	3 eV
Size of barriers	$5\ 10^{-10}$, $5\ 10^{-10}$, $6\ 10^{-10}$ m
Size of well	$15\ 10^{-10}$, $10\ 10^{-10}$ m
h	0.13
Penalization parameter	$\varepsilon = 0.01$
Discretization in voltage	100 points
Discretization in energy	200 points
Position of the well	$c_1 = 12\ 10^{-10}$, $c_2 = 30\ 10^{-10}$ m
Resonance depth	$(\varepsilon_1, \varepsilon_2) = (2.5, 2.1)$ eV
CPU time	84.99

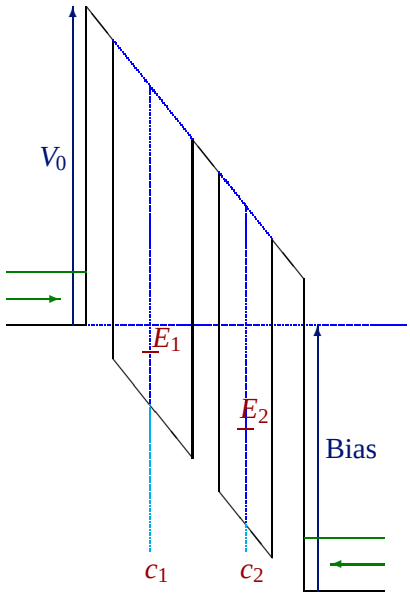

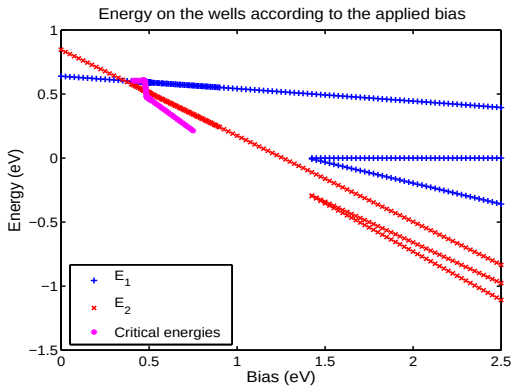

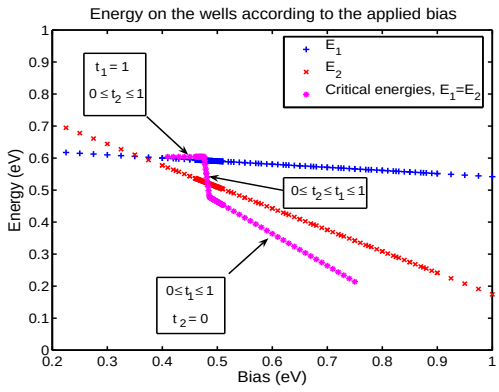

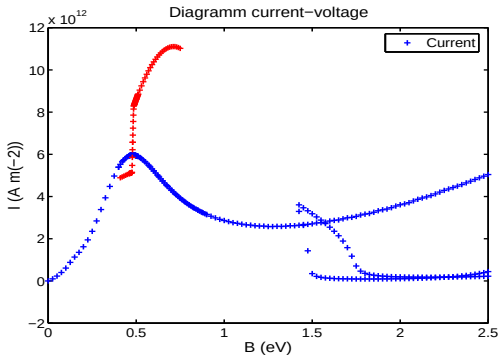

Figure 18: Critical solutions

9.2.5 Case 5.

The last example is a device with four wells. The bifurcation diagram (figure 19) in which only the generic cases were considered (no specific solution due to the crossing of resonant energies) suggests a complex interaction between the different resonant levels.

Donor density	$5\ 10^{26}$ m^{-3}
Fermi level E_F	0.716 eV
$B_{\min}$	0 eV
$B_{\max}$	3 eV
Height of barrier	3 eV
Size of barriers	$5\ 10^{-10}$, $5\ 10^{-10}$, $5\ 10^{-10}$, $5\ 10^{-10}$, $5\ 10^{-10}$ m
Size of well	$10\ 10^{-10}$, $10\ 10^{-10}$, $5\ 10^{-10}$, $5\ 10^{-10}$ m
h	0.13
Penalization parameter	$\varepsilon = 0.096$
Discretization in voltage	100 points
Discretization in energy	400 points
Position of the well	$c_1 = 11\ 10^{-10}$, $c_2 = 24\ 10^{-10}$, $c_3 = 39\ 10^{-10}$, $c_2 = 45\ 10^{-10}$, $c_5 = 55\ 10^{-10}$ m
Resonance depth	$(\varepsilon_1, \varepsilon_2, \varepsilon_3, \varepsilon_4) = (2.09, 2.24, 1.1, 1.68)$ eV
CPU time	528.63

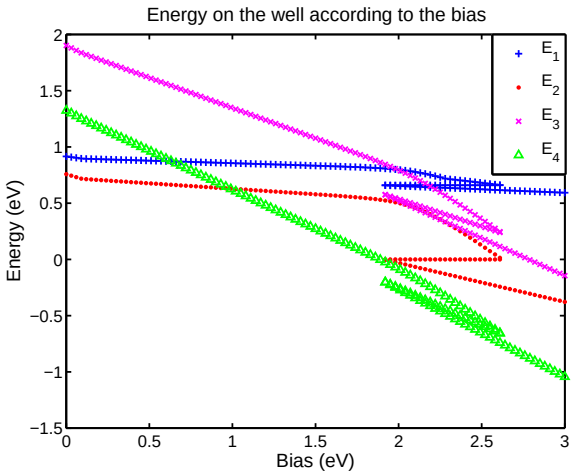

Figure 19: Solutions for a device with four wells

10 Conclusion.

These numerical experiments have shown on realistic cases that rather complex bifurcation diagramm can occur and are numerically accessible. This extends the previous works which were concerned with the hysteresis phenomenon (see for example [21, 37]). Our model permits to get very rapidly the shape of the bifurcation diagram. It relies on rigorous mathematical results concerned with the asymptotic regime of quantum wells in a semiclassical island, given in [32, 33]. Although the asymptotic model required some modifications in order to fit with the parameters of realistic devices, the numerical results happen

to be close to the ones of [26, 34, 35] based on a full treatment of the Schrödinger-Poisson system in the Landauer-Büttiker approach.

Those calculations must not be considered as final ones. Firstly, as it is discussed after Figure 17, the values of the current density have to be interpreted with some care. Secondly, our model does not take into account the nonlinear effect outside the quantum wells-barriers structure. Actually the space-charge effects in those area have been shown to be significant in some cases according to [27]. Finally the asymptotic model on which those calculations are based detects all the possible asymptotic solutions, without discriminating whether these solutions really exist or not. For example and even without considering the stability question, it is not clear that the detected critical solution of Figure 18 really exists or is replaced by some nonlinear beating effect.

Nevertheless these drawbacks are compensated by the rapidity of the method. This numerical approach can first be used in order to get an insight of the influence of the data (geometry and height of the barriers, donor density, temperature, applied bias ...) on the shape of bifurcation diagram. Finally, when several nonlinear solutions are possible, a Newton algorithm for complete simulations of the Schrödinger-Poisson system requires an initial guess. This approach provides it.

A Critical cases with two wells.

Relations (4.5)–(4.7) are derived here from analytical formulas of [32]. We keep the hypotheses and notations of Subsection 4.1.
In critical cases with two wells, the possible values of $t_1^{E_0}$ and $t_2^{E_0}$ are the limit points of quantities similar to

$$\tau_1^h = \cos^2\varphi^h \frac{\left|\theta_1^h\right|^2}{\kappa_0+\left|\theta_1^h\right|^2} + \sin^2\varphi^h \frac{\left|\theta_2^h\right|^2}{\kappa_0+\left|\theta_2^h\right|^2}, \tag{A.1}$$

$$\tau_2^h = \sin^2\varphi^h \frac{\left|\theta_1^h\right|^2}{\kappa_0+\left|\theta_1^h\right|^2} + \cos^2\varphi^h \frac{\left|\theta_2^h\right|^2}{\kappa_0+\left|\theta_2^h\right|^2}, \tag{A.2}$$

with $\kappa_0 > 0$ and

$$\theta_1^h = \kappa_1 \mathrm{e}^{\frac{\tilde{d}_h(c_r^{E_0},1)-\tilde{d}_h(0,c_\ell^{E_0})}{h}} \frac{1+\kappa_2\tan\varphi^h \mathrm{e}^{-\frac{\tilde{d}_h(c_\ell^{E_0},c_r^{E_0})}{h}}}{\tan\varphi^h+\kappa_3\,\mathrm{e}^{-\frac{\tilde{d}_h(c_\ell^{E_0},c_r^{E_0})}{h}}}, \tag{A.3}$$

$$\theta_2^h = \kappa_1 \mathrm{e}^{\frac{\tilde{d}_h(c_r^{E_0},1)-\tilde{d}_h(0,c_\ell^{E_0})}{h}} \frac{-\tan\varphi^h+\kappa_2\,\mathrm{e}^{-\frac{\tilde{d}_h(c_\ell^{E_0},c_r^{E_0})}{h}}}{1-\kappa_3\tan\varphi^h \mathrm{e}^{-\frac{\tilde{d}_h(c_\ell^{E_0},c_r^{E_0})}{h}}}. \tag{A.4}$$

The numbers κ_i are non vanishing real numbers and the quantity $\tilde{d}_h(x,y)$ is known up to some small error

$$\tilde{d}_h(x,y) = d_{Ag}(x,y;\tilde{\mathcal{V}}-E_0)+\varepsilon(x,y,h), \quad \text{with} \quad \lim_{h\to 0}\max_{x,y\in[0,1]}|\varepsilon(x,y;h)| = 0,$$

and where φ^h can take any value in $[0,\pi/2]$ without any additional information on V^h. We refer the reader to [32] pp 250–256 for details about this.
After possibly extracting a subsequence, several cases have to be considered :

1st case : $\varphi^{\mathbf{h}} \overset{\mathbf{h}\to\mathbf{0}}{\to} \varphi^{\mathbf{0}} \in (\mathbf{0}, \pi/\mathbf{2})$

This asymptotic behaviour of φ^h implies

$$\left|\theta_1^h\right| \sim |\kappa_1|\, e^{\frac{\tilde{d}_h(c_r^{E_0},1)-\tilde{d}_h(0,c_\ell^{E_0})}{h}} \frac{1}{\tan\varphi^0}, \tag{A.5}$$

$$\left|\theta_2^h\right| \sim |\kappa_1|\, e^{\frac{\tilde{d}_h(c_r^{E_0},1)-\tilde{d}_h(0,c_\ell^{E_0})}{h}} \tan\varphi^0. \tag{A.6}$$

Such a behaviour of θ_1^h, θ_2^h implies

$$1 \geq \lim_{n\to\infty} \tau_1^h \geq \lim_{n\to\infty} \tau_2^h \geq 0.$$

Indeed, we write

$$\tau_1^h \sim \cos^2\varphi^h \frac{\frac{1}{\tan^2\varphi^h}}{c^h + \frac{1}{\tan^2\varphi^h}} + \sin^2\varphi^h \frac{\tan^2\varphi^h}{c^h + \tan^2\varphi^h},$$

$$\tau_2^h \sim \sin^2\varphi^h \frac{\frac{1}{\tan^2\varphi^h}}{c^h + \frac{1}{\tan^2\varphi^h}} + \cos^2\varphi^h \frac{\tan^2\varphi^h}{c^h + \tan^2\varphi^h},$$

$$\text{with} \qquad c^h = \frac{\kappa_0}{|\kappa_1|^2\, e^{2\frac{d(c_r^{E_0},1)-d(0,c_\ell^{E_0})}{h}}}.$$

A simple factorization leads to

$$\tau_1^h - \tau_2^h = \frac{c_h \left(\cos^2\varphi^h - \sin^2\varphi^h\right)^2 \left(\cos^2\varphi^h + \sin^2\varphi^h\right)}{\left(c^h \sin^2\varphi^h + \cos^2\varphi^h\right)\left(c^h \cos^2\varphi^h + \sin^2\varphi^h\right)} \geq 0. \tag{A.7}$$

Three different possibilities can occur :

- $d_{Ag}(c_r^{E_0},1;\tilde{\mathcal{V}}-E_0) > d_{Ag}(0,c_\ell^{E_0};\tilde{\mathcal{V}}-E_0)$: With $\tilde{d}_h(x,y) = d_{Ag}(x,y;\tilde{\mathcal{V}}-E_0)+\varepsilon(x,y,h)$, this leads to

$$\lim_{h\to 0}\left|\theta_i^h\right| = +\infty, \qquad \lim_{h\to 0}\tau_i^h = 1,$$
$$\text{and finally} \qquad t_1 = t_2 = 1.$$

- $d_{Ag}(c_r^{E_0},1;\tilde{\mathcal{V}}-E_0) < d_{Ag}(0,c_\ell^{E_0};\tilde{\mathcal{V}}-E_0)$: This case leads to

$$\lim_{h\to 0}\left|\theta_i^h\right| = 0, \qquad \lim_{h\to 0}\tau_i^h = 0,$$
$$\text{and finally} \qquad t_1 = t_2 = 0.$$

- $d_{Ag}(c_r^{E_0},1;\tilde{\mathcal{V}}-E_0) = d_{Ag}(0,c_\ell^{E_0};\tilde{\mathcal{V}}-E_0)$: In this case, the asymptotic values of $t_1, t_2 \in [0,1]$ are undetermined with the constraint

$$1 \geq t_1 \geq t_2 \geq 0,$$

coming from (A.7). Note that here again the indeterminacy of t_1 and t_2 is replaced by the two constraints $\#J^{E_0} = 2$ and $d_{Ag}(c_r^{E_0},1;\mathcal{V}-E_0) = d_{Ag}(0,c_\ell^{E_0};\tilde{\mathcal{V}}-E_0)$.

2nd case : $\varphi^h \overset{h\to 0}{\to} 0$

This implies $\lim_{h\to 0}\tan\varphi^h = 0$, $\lim_{h\to 0}\cos\varphi^h = 1$, $\lim_{h\to 0}\sin\varphi^h = 0$ and therefore

$$\tau_i^h \sim \frac{\left|\theta_i^h\right|^2}{\kappa_0 + \left|\theta_i^h\right|^2}\,.$$

The quotient between $\left|\theta_2^h\right|$ and $\left|\theta_1^h\right|$ behaves according to

$$\frac{\left|\theta_2^h\right|}{\left|\theta_1^h\right|} \sim \left|\kappa_2\,\mathrm{e}^{-\tilde{d}_h(c_\ell^{E_0},c_r^{E_0})/h} - \tan\varphi^h\right| \left|\tan\varphi^h + \kappa_3\,\mathrm{e}^{-\tilde{d}_h(c_\ell^{E_0},c_r^{E_0})/h}\right| \overset{h\to 0}{\to} 0\,.$$

Here are two possibilities (after extraction of subsequences) :

- $\lim_{h\to 0}\left|\theta_2^h\right| \in (0,+\infty]$ and $\lim_{h\to 0}\left|\theta_1^h\right| = +\infty$: The first condition implies

  $$d_{Ag}(c_r^{E_0},1;\tilde{\mathcal{V}} - E_0) \geq d_{Ag}(0,c_\ell^{E_0};\tilde{\mathcal{V}} - E_0)$$

  and permits any value

  $$t_2 = \lim_{h\to 0}\tau_2^h \in (0,1]\,.$$

  Meanwhile the second condition implies

  $$t_1 = \lim_{h\to 0}\tau_1^h = 1\,.$$

- $\lim_{h\to 0}\left|\theta_1^h\right| \in [0,+\infty)$ and $\lim_{h\to 0}\left|\theta_2^h\right| = 0$: The first condition implies

  $$d_{Ag}(c_r^{E_0},1;\tilde{\mathcal{V}} - E_0) \leq d_{Ag}(0,c_\ell^{E_0};\tilde{\mathcal{V}} - E_0)$$

  and permits any value

  $$t_1 = \lim_{h\to 0}\tau_1^h \in [0,1)\,.$$

  Meanwhile the second condition implies

  $$t_2 = \lim_{h\to 0}\tau_2^h = 0\,.$$

3rd case : $\varphi^h \overset{h\to 0}{\to} \pi/2$

After replacing φ^h by $\pi/2 - \varphi^h$, it amounts to the second case.

Remark A.1. *The second case contains the limit points of case 1-third part. This suggests that all the values which satisfy* $1 \geq t_1 \geq t_2 \geq 0$ *can be achieved.*

References

[1] A. ARNOLD, Numerical absorbing boundary conditions for quantum evolution equation. *VLSI Design 6*, 1-4 (1998), 313–319.

[2] A. ARNOLD, Mathematical concepts of open quantum boundary conditions. *Transp. Theory Stat. Phys. 30*, 4-6 (2001), 561–584.

[3] M. BARO, N. BEN ABDALLAH AND P. DEGOND, A 1D coupled Schrödinger drift-diffusion model including collisions. *J. Comp. Phys. 203* (2005), 129–153.

[4] M. BARO, H. NEIDHARDT AND J. REHBERG, Current coupling of drift-diffusion models and Schrödinger–Poisson systems: dissipative hybrid models. *SIAM J. Math. Anal.* (2005).

[5] N. BEN ABDALLAH, On a multidimensional Schrödinger-Poisson scattering model for semiconductors. *J. Math. Phys. 41*, 7 (2000), 4241–4261.

[6] N. BEN ABDALLAH, P. DEGOND AND P. A. MARKOWICH, On a one-dimensional Schrödinger-Poisson scattering model. *Z. Angew. Math. Phys. 48*, 1 (1997), 135–155.

[7] N. BEN ABDALLAH AND O. PINAUD, Multiscale simulation of transport in an open quantum system: Resonances and WKB interpolation. *To appear J. Comp. Phys.* (2005).

[8] M. BÜTTIKER, Y. INRY, R. LANDAUER AND S. PINHAS, Generalized many-channel conductance formula with application to small rings. *Phys. Rev. B 31* (1985), 6207–6215.

[9] P. CAUSSIGNAC, J. DESCLOUX AND A. YAMNAHAKKI, Simulation of some quantum models for semiconductors. *Math. Models Methods Appl. Sci. 12*, 8 (2002), 1049–1074.

[10] Z. CHEN, A finite element method for the quantum hydrodynamic model for semiconductor devices. *Comput. Math. Appl. 31*, 7 (1996), 17–26.

[11] Z. CHEN, B. COCKBURN, C. L. GARDNER AND J. W. JEROME, Quantum hydrodynamic simulation of hysteresis in the resonant tunneling diode. *J. Comput. Phys. 117*, 2 (1995), 274–280.

[12] F. CHEVOIR AND B. VINTER, Scattering assisted tunneling in double barriers diode: scattering rates and valley current. *Phys. Rev. B 47* (1993), 7260–7274.

[13] P. DEGOND, F. MEHATS AND C. RINGHOFER, Quantum energy transport and drift diffusion models. *J. Stat. Phys. 118*, 3–4 (2005), 625–665.

[14] W. R. FRENSLEY, Boundary conditions for open quantum systems driven for equilibrium. *Rev. Mod. Phys. 62*, 3 (1990), 745–791.

[15] C. GÉRARD AND A. MARTINEZ, Semiclassical asymptotics for the spectral function of long-range Schrödinger operators. *J. Funct. Anal. 84*, 1 (1989), 226–254.

[16] V. GRECCHI, A. MARTINEZ AND A. SACCHETTI, Double well Stark effect: crossing and anticrossing of resonances. *Asymptotic Anal. 13*, 4 (1996), 373–391.

[17] V. GRECCHI, A. MARTINEZ AND A. SACCHETTI, Destruction of the beating effect for a nonlinear Schrödinger equation. *Comm. Math. Phys. 227*, 1 (2002), 191–209.

[18] B. HELFFER, *Semi-classical analysis for the Schrödinger operator and applications*, vol. 1336 of *Lecture Notes in Mathematics*. Springer-Verlag, Berlin, 1988.

[19] B. HELFFER AND J. SJÖSTRAND, Résonances en limite semi-classique. *Mém. Soc. Math. France (N.S.) 24-25* (1986), iv+228.

[20] P. D. HISLOP AND I. M. SIGAL, *Introduction to spectral theory*, vol. 113 of *Applied Mathematical Sciences*. Springer-Verlag, New York, 1996. With applications to Schrödinger operators.

[21] G. JONA-LASINIO, C. PRESILLA AND J. SJÖSTRAND, On Schrödinger equations with concentrated nonlinearities. *Ann. Physics 240*, 1 (1995), 1–21.

[22] J. KASTRUP, R. KLANN, H. GRAHN, K. PLOOG, L. BONILLA, J. GALÁN, M. KINDELAN, M. MOSCOSO AND R. MERLIN, Self-oscillations of domains in doped gaas-alas superlattices. *Phys. Rev. B 52* (1995), 13761–13764.

[23] W. KIRSCH AND B. SIMON, Universal lower bounds on eigenvalue splittings for one-dimensional Schrödinger operators. *Comm. Math. Phys. 97*, 3 (1985), 453–460.

[24] A. M. KRIMAN, N. C. KLUKSDAHL AND D. K. FERRY, Scattering states and distribution functions for microstructures. *Phys. Rev. B 36* (1987), 5953–5959.

[25] R. LANDAUER, Spatial variation of currents and fields due to localized scatterers in metallic conduction. *IBM J. Res. Develop. 1* (1957), 223–231.

[26] S. E. LAUX, A. KUMAR AND M. V. FISCHETTI, Analysis of quantum ballistic electron transport in ultra-small semiconductor devices including space-charge effects. *J. Appl. Phys. 95* (2004), 5545–5582.

[27] P. MOUNAIX, O. VANBÉSIEN AND D. LIPPENS, Effects of cathode space layer on the current-voltage characteristics of resonant tunneling diodes. *Appl. Phys. Letter 57*, 8 (1990), 1517–1519.

[28] F. NIER, Schrödinger-Poisson systems in dimension $d \leq 3$: the whole-space case. *Proc. Roy. Soc. Edinburgh Sect. A 123*, 6 (1993), 1179–1201.

[29] F. NIER, A variational formulation of Schrödinger-Poisson systems in dimension $d \leq 3$. *Comm. Partial Differential Equations 18*, 7-8 (1993), 1125–1147.

[30] F. NIER, The dynamics of some quantum open systems with short-range nonlinearities. *Nonlinearity 11*, 4 (1998), 1127–1172.

[31] F. NIER AND Y. PATEL, Nonlinear asymptotics for quantum out of equilibrium 1d systems: Reduced models and algorithms. t. Conference "Multiscale methods in quantum mechanics and experiments", Eds., Accademia dei Lincei Roma.

[32] Y. PATEL, *Développements de modèles macroscopiques pour des systèmes quantiques nonlinéaires hors-équilibre*. Thèse de doctorat, Université de Rennes I, 2005.

[33] Y. PATEL, Steady states of 1D-Schrödinger-Poisson systems with quantum wells I. *in preparation* (2005).

[34] O. PINAUD, Transient simulations of a resonant tunneling diode. *J. App. Phys. 92*, 4 (2002), 1987–1994.

[35] O. PINAUD, *Analyse mathématique et numérique de quelques problèmes de transport dans les nanostructures*. Thèse de doctorat, Université Paul Sabatier de Toulouse, 2003.

[36] R. PINNAU AND A. UNTERREITTER, The stationary current-voltage characteristics of the quantum drift-diffusion model. *SIAM J. Numer. Anal. 37*, 1 (1999), 211–245.

[37] C. PRESILLA AND J. SJÖSTRAND, Transport properties in resonant tunneling heterostructures. *J. Math. Phys. 37*, 10 (1996), 4816–4844.

[38] M. REED AND B. SIMON, *Methods of modern mathematical physics. IV. Analysis of operators*. Academic Press [Harcourt Brace Jovanovich Publishers], New York, 1978.